

In presenting this thesis in partial fulfillment of the requirements for an advanced degree at Idaho State University, I agree that the Library shall make it freely available for inspection. I further state that permission for extensive copying of my thesis for scholarly purposes may be granted by the Dean of the Graduate School, Dean of my academic division, or by the University Librarian. It is understood that any copying or publication of this thesis for financial gain shall not be allowed without my written permission.

Signature _____

Date _____

Trace Element Analysis of Slag and Coal Materials Using Photon Activation
Analysis

by

Nathaniel W. Gardner

A thesis submitted

in partial fulfillment of the requirements

for the degree of Masters of Science in the

Department of Nuclear Engineering

Idaho State University

Spring 2018

©2018 – Nathaniel W. Gardner

All rights reserved.

To the Graduate Faculty:

The members of the committee appointed to examine the thesis of NATHANIEL W. GARDNER find it satisfactory and recommend that it be accepted.

Dr. D. Dale,
Major Advisor

Dr. C. Pope,
Committee Member

Dr. M. Ellis,
Graduate Faculty Representative

For my Grandfather

Acknowledgements

I would like to thank my parents for always believing in me, and pushing me to be more than I am today. I would also like to thank my Advisor, Dr. Daniel S. Dale, for without him and a series of fortunate events this opportunity would not have existed. Finally I would like to thank Jeff Burggraf and my friends for their assistance in producing this thesis.

TABLE OF CONTENTS

List of Figures.....	viii
List of Tables.....	x
Abstract.....	xii
1 Introduction	1
1.1 Technique Behind Photon Activation Analysis	1
1.2 History of Photon Activation Analysis	2
1.3 Advantages of Photon Activation Analysis	3
2 Relevant Theory	4
2.1 Bremsstrahlung	4
2.2 Coulomb Barrier	5
2.3 Giant Dipole Resonance	6
2.4 Long Lived States	8
3 Experiment Methodology	10
3.1 Basis of the Experiment	10
3.2 Mining Slag.....	12
3.3 Coal, Coal Ash and Fly Ash	17
4 Results.....	19
4.1 Slag	19
4.2 Coal, Coal Ash and Fly Ash	23
4.3 Mathematical Analysis Derivation of Ratio Method	30
4.3.1 Example Calculation for Sample A	32

4.4	Extrapolation Method	34
4.5	Mathematical Derivation of Extrapolation Method.....	38
4.6	Missing Masses	41
5	Conclusions.....	53
5.1	Slag Conclusion	53
5.2	Coal, Coal Ash and Fly Ash Conclusions.....	53
5.3	Missing Elements Conclusions	54
	Bibliography	56

List of Figures

1	A schematic of the Coulomb potential vs. separation distance for a proton-proton interaction showing the Coulomb barrier	6
2	A graph of the photoreaction cross section vs. energy which shows the various peaks of cumulative excitation with a very large peak representing the Giant Dipole Resonance (GDR)	7
3	A simplified image of a nucleus losing energy through an isobaric and then an isomeric transition	9
4	The irradiation sample arrangement intended to maximize flux as seen from a top down and sideways orientation.....	14
5	Schematic of the high purity germanium detector end cap.....	15
6	Two part image showing first the attachment of a sample of coal ash to the apparatus used for holding samples during counting. The second image shows the placement of the holding apparatus relative to the HPGe detector end cap	16
7	The timeline used to illustrate t_0 , t_1 and t_2 for use in the derivations	30
8	The linear relationship between scandium and activity of 1157 keV line in coal ash.....	37
9	The linear relationship between yttrium and activity of 898 keV line in coal ash	37
10	The linear relationship between europium and activity of 963 keV line in coal ash.....	38
11	Image showing the 1596 keV peak in Dr. Dale's slag countcount.....	41
12	Image showing the missing 1596 keV peak in the slag sample A count.....	42
13	Image showing the missing 1596 keV peak in the slag sample B count	42
14	Image showing the missing 1596 keV peak in the slag sample C count	43
15	Image showing the missing 1596 keV peak in the slag sample D count.....	43

16	Image showing the 963 keV peak in Dr. Dale's coal ash count	44
17	Image showing the 963 keV peak in the coal ash sample A3 count.....	44
18	Image showing the 963 keV peak in the coal ash sample A2 count.....	45
19	Image showing the missing 963 keV peak in the coal ash sample A1 count	45
20	Image showing the missing 963 keV peak in a second coal ash sample A1 count	46
21	Image showing the 898 and 1836 keV peaks in Dr. Dale's coal ash count.....	47
22	Image showing the 898 keV peak in the coal ash sample A3 count.....	48
23	Image showing the 898 keV peak in the coal ash sample A2 count.....	48
24	Image showing the 898 keV peak in the coal ash sample A1 count.....	49
25	Image showing the missing 898 keV peak in a second coal ash sample A1 count	49
26	Image showing the 145 and 166 keV peaks in Dr. Dale's fly ash count	50
27	Image showing a missing 145 keV peak and a showing 166 keV peak in fly ash sample F3 count	51
28	Image showing the missing 145 and 166 keV peaks in fly ash sample F2 count.....	51
29	Image showing the missing 145 and 166 keV peaks in fly ash sample F1 count.....	52
30	Image showing the missing 145 and 166 keV peaks in second fly ash sample F1 count..	52

List of Tables

1	Summary of slag and nickel count data created by MPA program	21
2	Summary of slag and nickel initial activities calculated by Eqn. 2.3	21
3	Summary of slag and nickel mass information sorted by sample.....	21
4	Summary of normalized flux received by slag samples as calculated by Eqn. 3.2	22
5	Summary of rare earth element mixture information, mass of mixture added to samples and scandium added to samples as calculated by Eqn. 6.1	22
6	Final calculated concentrations of scandium and yttrium in slag as calculated by Eqn. 5.3.....	23
7	Summary of coal, coal ash, fly ash and nickel mass information sorted by sample.....	24
8	Summary of coal and nickel count data created by MPA program	24
9	Summary of coal and nickel mass information sorted by sample	24
10	Summary of rare earth element mixture mass information needed for Eqn. 6.1	25
11	Summary of scandium added to coal as calculated by Eqn. 6.1	25
12	Final calculated concentration of scandium in coal as calculated by Eqn. 5.3	25
13	Summary of coal ash and nickel count data created by MPA program.....	26
14	Summary of coal ash and nickel mass information sorted by sample	26
15	Summary of scandium and yttrium added to coal ash as calculated by Eqn. 6.1	27
16	Final calculated concentrations of scandium and yttrium in coal ash as calculated by Eqn. 5.3	27
17	Summary of fly ash and nickel count data created by MPA program	28
18	Summary of fly ash and nickel mass information sorted by sample	28
19	Summary of scandium and yttrium added to fly ash as calculated by Eqn. 6.1	29

20	Final calculated concentrations of scandium and yttrium in fly ash as calculated by Eqn. 5.3.....	29
21	Comparison of coal ash internal line activity ratios to nickel line activity ratios.....	36
22	Final calculated concentrations of scandium, yttrium and europium in coal ash using the extrapolation method.....	38

Trace Element Analysis of Slag, Coal and Coal By-Products Using Photon Activation Analysis

Thesis Abstract – Idaho State University (2018)

Photon activation analysis has long been used as a method to identify unknown elements in a sample. The technique relies upon creating high energy photons via bremsstrahlung from a particle accelerator which then undergo photonuclear reactions in a target sample. The sample is left in an excited state which can decay via gamma ray emission; the gamma emissions can be analyzed using gamma spectroscopy techniques. This research focused on the use of photon activation analysis to perform a measurement of trace element quantities of known elements in several samples. A 25 MeV linear accelerator was used to create the activation bremsstrahlung. The photons were directed at samples of mining slag, coal, coal ash, and fly ash. The activated samples were then analyzed using gamma ray detectors and the Multi-Purpose Analysis (MPA) program. Finally, the resulting peaks were compared with known standards to extract mass information down to the microgram level.

Chapter 1

Introduction

1.1 Technique Behind Photon Activation Analysis

Photon Activation Analysis (PAA) is similar to neutron activation analysis in that they both are based upon a reaction with the nucleus of an atom. However, while neutron activation analysis focuses on adding neutrons to the atom or replacing protons with neutrons via (n,p), photon activation analysis instead removes nucleons from the atom [1]. The nucleons are removed through a high energy photon causing a nuclear reaction by scattering or being absorbed by the nucleus. The removal of a nucleon leaves the atom in an excited state which can decay and produce gamma emissions.

The gamma emissions of the excited nuclei can then be examined using the gamma spectroscopy technique, which was originally developed to analyze naturally radioactive sources. Radioactive nuclei, or radionuclides, very commonly emit gamma rays with energies ranging from a few keV up to 10's of MeV [1]. These decays emit a discrete gamma line, or lines, corresponding to the energy lost in transitioning from the higher energy state to a lower one. Due to the limiting physics of these transitions, there are very few elements which emit a similar line and none which emit an identical spectrum. Since each of these spectra are unique, the radioactive isotopic source can be identified by its unique gamma ray fingerprint. [1]

The radioactive element that is identified by the gamma emission is not the original nuclide in the sample. Instead, it is a nuclide created by the photonuclear reaction in the target. Once the

daughter element is identified, the original element's identity can be determined. The identity can be determined by applying an understanding of the photonuclear reaction thresholds and branching ratios to eliminate the possible candidates until the element of interest in the sample is finally identified.

1.2 History of Photon Activation Analysis

The first PAA applications were reported to have been in the 1950's, however the first beryllium detections by photodisintegration were performed in the late 1930's. Thus, PAA was developed at approximately the same time as neutron activation analysis [1]. Due to the lack of high power accelerators in the 50's, the early applications of PAA were limited to very light elements and a few fissile nuclides.

Very light elements have to be analyzed using the energy spectra of the beta particle emitted because they do not have the necessary binding energy to produce gamma rays during their decay. The parent element of the decay is much harder to identify since there is no unique beta energy associated with any beta decay due to the random sharing of kinematic energy between the beta particle, parent nucleus and the neutrino. This limitation was a severe hindrance on the applicability of PAA.

However, in the 60's the potential of photon activation analysis was finally realized due to the availability of linear accelerators and high powered electron accelerators such as the betatron and microtron. The higher electron beam energies allowed higher energy gamma ray sources to be achieved via bremsstrahlung. The higher energy gamma ray sources were needed due to the higher threshold energies of the larger elements. This led to the expansion of the PAA technique to include elements with much higher Z values. The greatest advantage of the expansion is higher Z

elements have enough energy associated with their decay to produce gamma rays, thus allowing PAA to be combined with gamma ray spectroscopy.

1.3 Advantages of Photon Activation Analysis

Photon activation analysis works in a similar way to other activation techniques in that it tends to be non-destructive, and work via a nuclear reaction that creates an unstable isotope. Despite these similarities, PAA has some distinct advantages over other activation techniques, such as neutron activation analysis.

In neutron activation analysis the facility cost is extremely high due to the tight regulations surrounding the nuclear industry. The cost of a TRIGA reactor is on the order of 10 million dollars [16]. This is in sharp contrast with the cost of the particle accelerators used in PAA, which are significantly cheaper on the 10 thousand dollars range [17]. The personnel cost of particle accelerators are also lower due to the amount of personnel needed to run the facility as well as the amount of training required.

Photon activation analysis also benefits from a very rapid analysis time. There are only two factors that limit this time. The first of these two factors is beam time, both in waiting for an available accelerator and in the duration of irradiation needed to achieve the desired activity. The second factor is counting time. The longer the half-life of the isotope being interrogated the longer the sample needs to be counted for accurate results.

Chapter 2

Relevant Theory

2.1 Bremsstrahlung

Bremsstrahlung is a German word coined by the theoretical physicist Arnold Sommerfeld in 1909. It is directly translated as “braking radiation” and is an apt name for the effect it describes. This phenomenon applies to charged particles which are traveling close to the speed of light, or in other words are relativistic. The charged particles of most interest for this effect are electrons and positrons due to their small masses. Since they are so light these particles require the least amount of energy to accelerate to relativistic velocities in a particle accelerator [20].

When an extremely high velocity electron comes close to a high Z nucleus it interacts with the Coulomb field of the protons. The interaction with the Coulomb field of the nucleus creates an unbalanced force on the electron resulting in an acceleration. This acceleration can cause anywhere from a minor deflection of the electrons' trajectory, to causing the electron to completely stop. This acceleration causes the electron to lose some of its energy which is radiated as electromagnetic radiation. The energy spectrum of the bremsstrahlung range from 0 eV to just under the maximum energy (E_{\max}) of the relativistic particle. This spectrum has a peak at approximately one-third of E_{\max} for a thick bremsstrahlung converter [21].

In photon activation analysis there is a need for high energy gamma rays. When these gamma rays impinge upon the nucleus of an atom they can be absorbed causing the nucleus to

become unstable and subsequently radioactively decay. The bremsstrahlung created by a high energy particle accelerator shooting electrons into a high Z converter is an intense source of these needed gamma rays.

2.2 Coulomb Barrier

The Coulomb barrier is a well understood phenomenon that plays a role in many nuclear reactions such as alpha decay and fusion. The Coulomb barrier results in the force that positive particles experience as they get close to the surface of the positively charged nucleus. As shown in Fig. 1 the Coulomb barrier falls off with distance ($1/r$) and has a finite peak near the nuclear radius ($r_n = 1.2\text{fm} \cdot A^{1/3}$) [22]. Within the nucleus the strong force takes over and instead of being repulsive the overall force becomes attractive.

This barrier is important to the considerations of PAA because it plays a very large role in determining the threshold of any photonuclear reactions that emit a charged particle. The barrier holds charged particles out, but it also holds charged particles in by the same mechanism. Thus often (γ, p) requires more energy than (γ, n) , so certain desired reactions can be selected for based on the maximum energy of the electron beam.

2.3 Giant Dipole Resonance

The giant dipole resonance (GDR) is a phenomenon related to the gamma ray absorption of nuclei. The GDR typically occurs between 13 and 25 MeV and the peak in photoabsorption cross section decreases as the mass of the nucleus increases. The width of the GDR is related to

the sub-structure of the nucleus, being greatest for non-closed-shell nuclei. The GDR is a peak in the photo-absorption cross section of the nucleus for a specific energy range. [23].

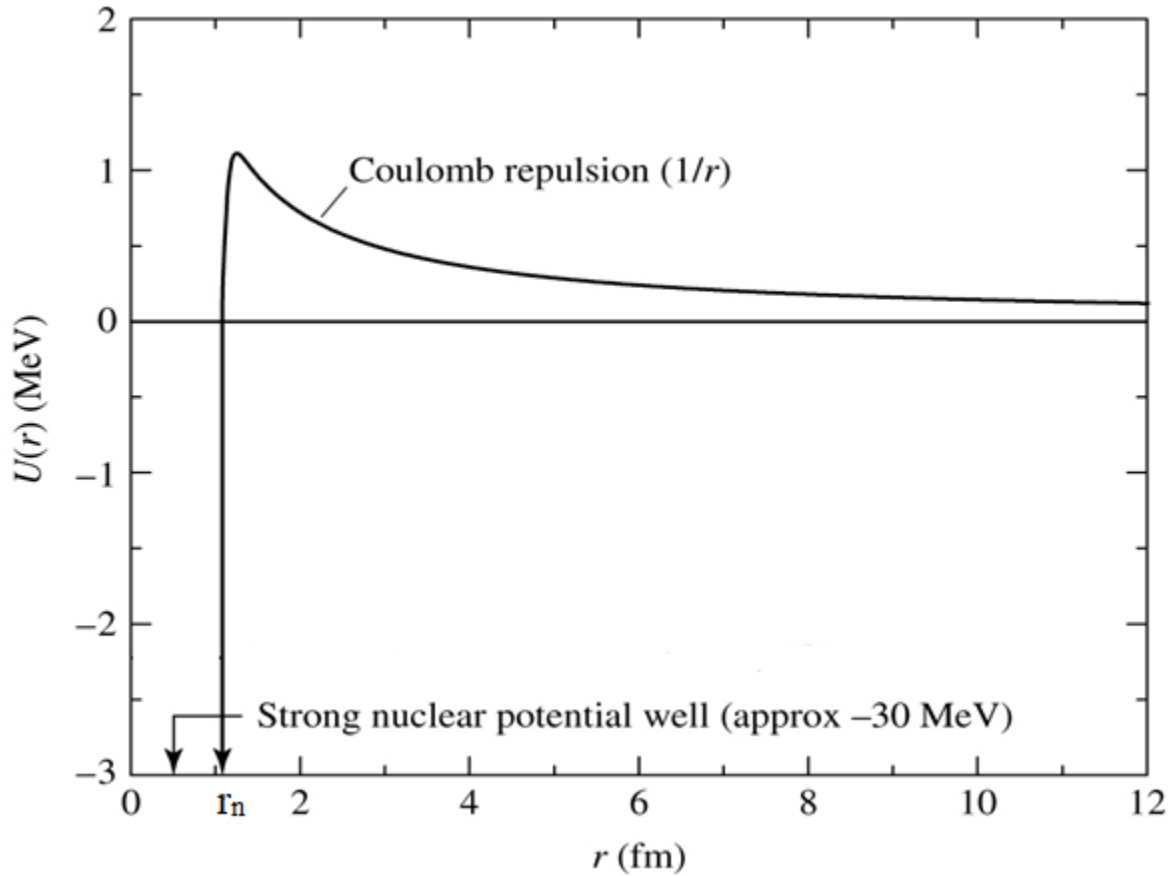
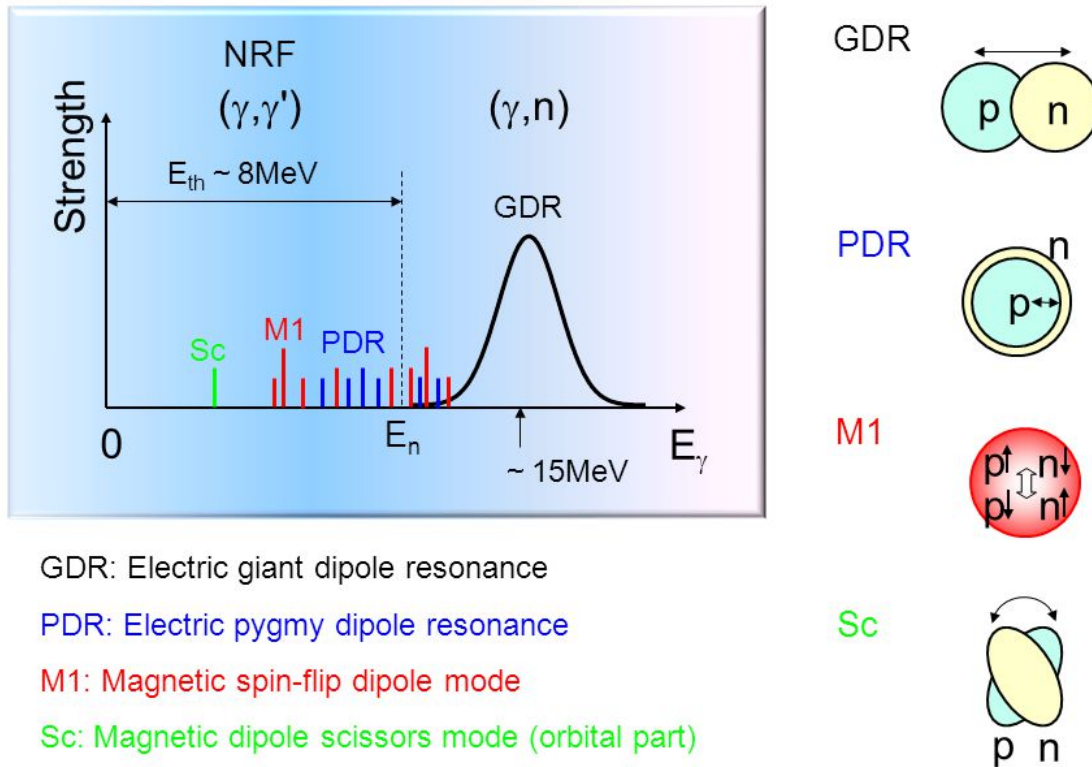


Fig. 1: Coulomb Barrier

The GDR is, as the name implies, a resonance in the collective excitation of nucleons in the nucleus, or more specifically the oscillation of neutrons against protons as shown in Fig. 2 [24]. As such it is most aptly described by the collective model, however the shell model can also somewhat predict the GDR. Being discovered in 1947 by Baldwin and Klaiber, the GDR is one of the earliest known collective effects in nuclei.

Strength Distribution of Dipole Excitation



GDR: Electric giant dipole resonance

PDR: Electric pygmy dipole resonance

M1: Magnetic spin-flip dipole mode

Sc: Magnetic dipole scissors mode (orbital part)

Fig. 2: Giant Dipole Resonance (GDR).

The GDR plays an important role in PAA due to the significant photonuclear reaction cross sections. With correct application of the endpoint electron beam energy the gamma beam energy can be made to have maximal overlap with the GDR energy range. This is another tool experimenters can implement to focus on the reaction of interest. In order to maximize the effect of the GDR, the maximum energy of the beam should be three times larger (for thick bremsstrahlung converters) than the energy of the GDR peak. This relationship ensures the maximum gamma flux at the GDR due to the energy distribution of the bremsstrahlung photons.

2.4 Long Lived States

Most nuclear half-lives (10^{-12} seconds) are much shorter than the blink of an eye. This extremely short duration means there is no chance to place them in front of a detector before all the decay reactions have already occurred. Luckily for PAA there are excitations known as metastable states [25]. A metastable state describes a nucleus with an excited state that is many hundreds of times longer than the typically expected half-life.

Most delayed transitions arise when quantum mechanical selection rules make direct gamma emission unlikely. In these cases, the nucleus often undergoes beta decay, which is typically a slow process. The daughter nucleus of the beta decay then often emits gamma rays which can be detected. This process can become further delayed if the daughter is in an isomeric state (as shown in Fig.3).

There are three different types of isomeric states, sometimes referred to as isomers. The first kind of isomer is called a K-isomer and is caused by a large difference in the angular momentum between the parent and daughter state. Due to the conservation of angular momentum the state cannot easily transition thus leading to a long half-life. The second type of isomer is known as either a shape isomer or a fission isomer. This is caused by the nucleus becoming trapped in a slightly stable shape in between two unstable shapes. The last isomer is a spin isomer. This isomer is caused by a large mismatch in spin between the parent and daughter state. The isomeric transitions of most relevance to PAA involve spin isomers. These isomers occur at far higher rates than the other types.

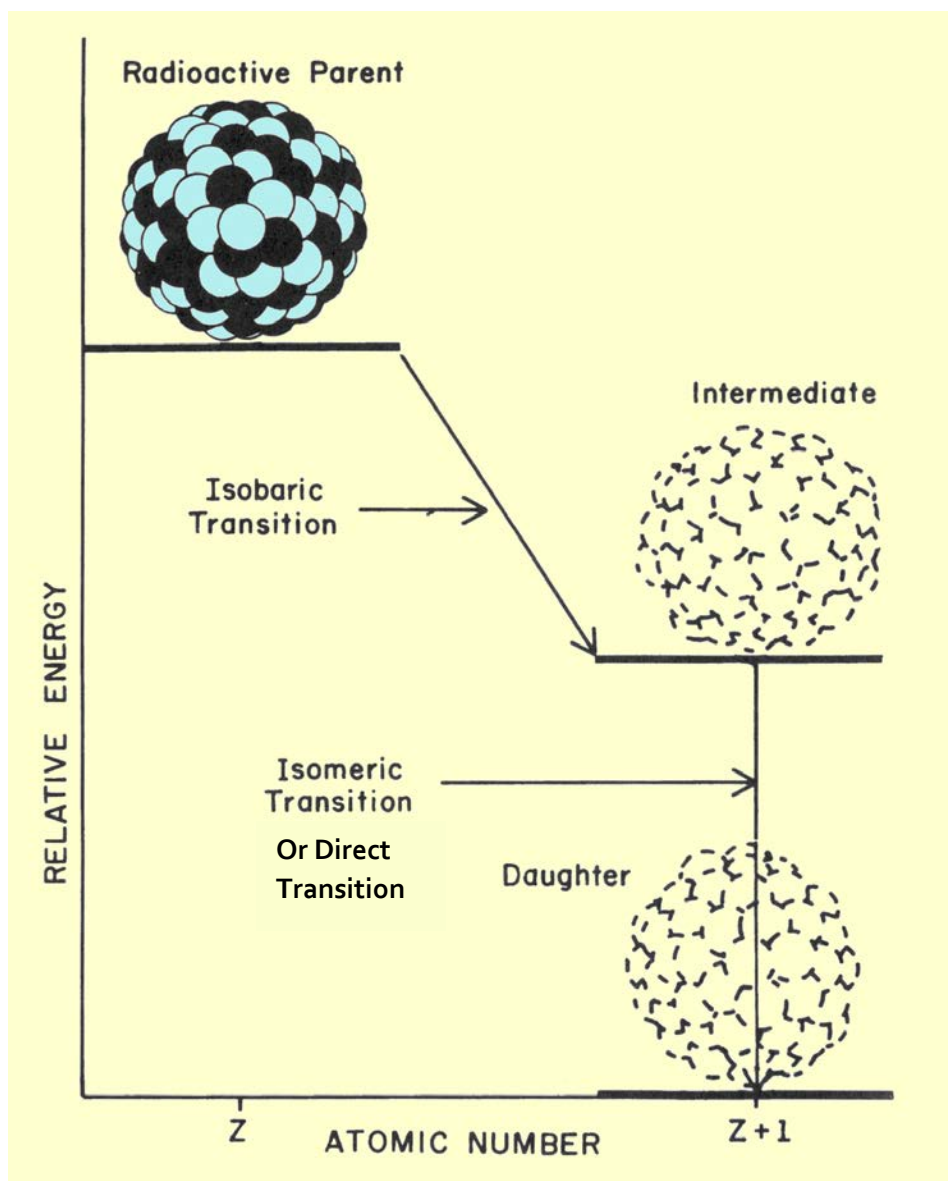


Fig. 3: Beta delayed decay.

Chapter 3

Experiment Methodology

3.1 Basis of the Experiment

The goal of this experiment is to validate the use of Photon Activation Analysis (PAA) to perform a timely, low cost, trace element analysis. This will simultaneously prove the efficacy of the technique for this application being performed at the Idaho Accelerator Center and provide information to the mining company which supplied the slag.

The experiment is building upon previous work by Dr. Daniel Dale in which he irradiated mining slag, coal, coal ash, and fly ash samples. Upon examining the gamma lines of the samples, several significant signals were found. The first of these signals was a line at 898 keV and another at 1836 keV. These two lines strongly suggested yttrium was in the samples. A suspect gamma peak at 1596 keV gave the possibility of cerium. A strong peak at 1157 keV lead to the potential of scandium. In coal ash a signal of 963 keV seemed to indicate very small amounts of europium. Lastly a 165 keV peak had a small possibility of being praseodymium.

All but one of the elements potentially detected by Dr. Dale are known as ‘technology metals’. This term was coined by a man named Jack Lifton in 2007, but has become a widely used phrase [18]. This phrase refers to a group of rare metals that are required for producing our ever advancing technologies. As these advanced technologies become more popular and wide spread the demand, and thus price, of these metals will only increase.

Mining slag is a by-product from the refining process and is considered a waste material. Slag is usually stored in a pond on site, or dried and stacked in large piles [14,15]. If there are significant concentrations of rare earth elements in the mining slag, it could be further refined

thereby increasing the profits of the mine. This would not only provide more access to these rare ‘technology metals’, it would also help alleviate the staggering environmental concerns these massive waste piles represent.

Every year, the United States burns millions of tons of coal to produce about 30% of the total electricity generation. In 2017 the U.S. consumed 204 million short tons of coal, with about 94% of that being used by the energy sector [19]. Due to the sheer mass of coal burned, the smallest concentrations of trace elements in coal could result in large quantities of the element being released. Not only is this an environmental concern, it is also a monetary one. Some of the trace elements in coal are valuable enough that coal burning by-products could potentially be reprocessed instead of discarded. These trace elements can be concentrated in the resulting ash, volatilized and later deposited with the fly ash in the stack, or released into the air. The objective of this experiment is to determine some rare earth element concentrations and approximate where those elements go during the burning process.

3.2 Mining Slag

If the rare earth elements in the slag are not detected it should not be assumed that they are not there. They could be in the slag at concentrations below the minimum detectable limit of the lab equipment. “Typically the detection limits - assuming a purely instrumental analysis - lie between 0.01 and 1 microgram.” [1]. The minimum detectable limit depends mainly upon the sensitivity of the detector. The detectable limit requires that the count rate of the line being interrogated must be approximately 3 times the count rate of the background in order to be considered statistically significant [7,8]. Another consideration of detection is that, while activating the rare earth elements, another element in the sample matrix is activated and produces

the same daughter product as one of the rare earth elements. This will create first order interference in the form of competing signals, which will complicate or invalidate the determination of the concentration of the rare earth element that is being measured. To minimize the chances of creating this effect, the electron beam energy will be set at 20 MeV [1]. At this energy level it will be highly unlikely that any elements in the sample will undergo a reaction which ejects a charged particle; (γ,γ') , (γ,n) and $(\gamma,2n)$ will be the primary reactions induced in the target sample.

A mixture of the rare earth elements being investigated was created to act as an internal standard. An internal standard is essential because the cross sections of these elements are largely unknown. This mixture started out on a scale which was zeroed out while a measuring tray was on it. This tray then had a quantity of europium added to it, the mass was recorded, and the scale was re-zeroed. After that an amount of cerium was added, its mass was recorded, then praseodymium was added. The amount of praseodymium added was determined by taking the new reading on the scale and subtracting it from the reading which was only cerium's mass. This same step was then repeated with yttrium and this new reading was subtracted from the old value of the praseodymium and cerium mixture's mass. Finally, the procedure was repeated one last time to add an amount of scandium. The mixture was stirred, and elements pre-ground, in an effort to achieve as close to a homogeneous powder as possible. This mixture was created with the intention of containing 0.2 grams of each element, but because these elements exist in oxide states, this meant that more than 0.2 grams of the oxide needed to be added to reach the 0.2 gram target. The exact quantities added to the mixture are recorded in table 5.

The target samples were prepared by taking a large homogenous bag of mining slag and very carefully measuring approximately 1 gram quantities of it into small glass vials. This was done by zeroing out a scale, which had a measuring tray on it, and adding slag to the measuring

tray to approximately a 1 gram amount. After that the tray was replaced with a glass vial and the scale was re-zeroed. Then the vial was removed from the scale and the slag was carefully poured into it, after which it was placed back on the scale. The reading on the scale now represented the exact quantity of slag contained within the vial.

To create a control, one vial was left as purely slag. Ever increasing amounts of the mixture of rare earth elements was added to the other vials in order to establish a relationship of activity to mass of element in the sample. The mixture was added to the vials using an identical procedure to the one used to add the slag. A letter was written on the side of each of the four vials, from A to D, to aid in identification and they were sealed with Parafilm. Tables 3 and 5 have listed the quantities of slag and mixture contained in each vial.

Once the samples were fully prepared, they were arranged in a fixed geometry, as shown in Fig. 4, and secured together with Kapton tape. This was done with the goal of maximizing the flux each target received. The sample arrangement was placed directly in front of the bremsstrahlung converter to maximize the flux the samples received.

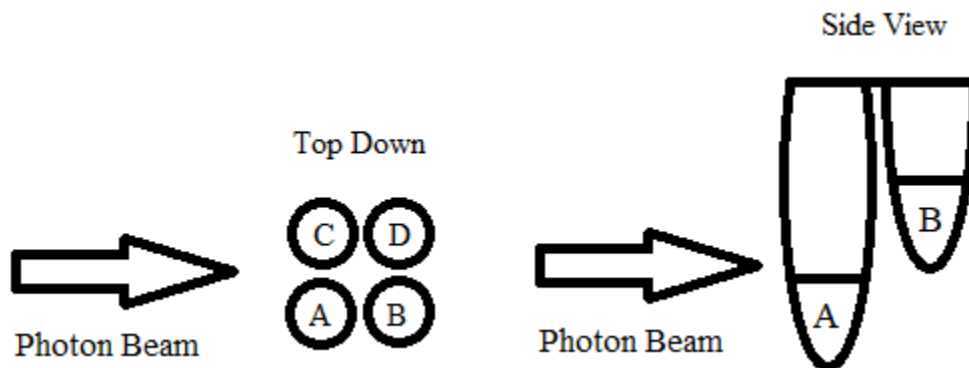


Fig. 4: Sample arrangement for irradiation.

The gamma flux cone resulting from the bremsstrahlung of the accelerator has a slowly varying energy distribution and a rapidly varying flux distribution [1]. In order to monitor and

calibrate for the different flux each target receives, they were wrapped in a small, measured mass of nickel foil. The flux received by a sample is proportional to the activity of the nickel foil wrapped around that sample scaled down by the mass of the foil. By correlating the activity and mass of the foils between two samples, a ratio of the flux received between the two samples can be achieved. The foil was weighed in a plastic measurement tray on the same electronic scale used to weigh the mixtures and slag, and it was then affixed to the corresponding vial using Kapton tape.

Natural nickel contains about 68% of the isotope Ni-58. When subjected to the gamma rays generated during this experiment the Ni-58 undergoes a reaction of $^{58}\text{Ni}(\gamma, n)^{57}\text{Ni}$. The photon-activation product, Ni-57, produced by the (γ, n) reaction on Ni-58, cannot be produced from any other element at bombarding energies less than about 45 MeV. Ni-57 is radioactive with a half-life of 35.6 hours, when it decays a unique set of gamma rays are emitted, including a gamma ray with an energy of 1377 keV.

Post irradiation, the samples were processed by the health physicist at the Idaho Accelerator Center (IAC). The health physicist transferred the contents of each vial to a plastic bag which was labelled with its corresponding sample identification letter. The nickel foils were also removed from the vials and transferred to their own marked bags. This allowed counting of each of the slag and nickel samples separately in order to minimize competing signals and - more importantly - dead time. The counting was done with the Ortec model number SGD-GEM-50180P-S high energy resolution, high purity germanium (HPGe), gamma ray spectrometer shown in Fig. 5. This detector sends the information to a computer where the gamma spectrometry analysis is done using a software tool called MPA.

End Cap = 83 mm diameter

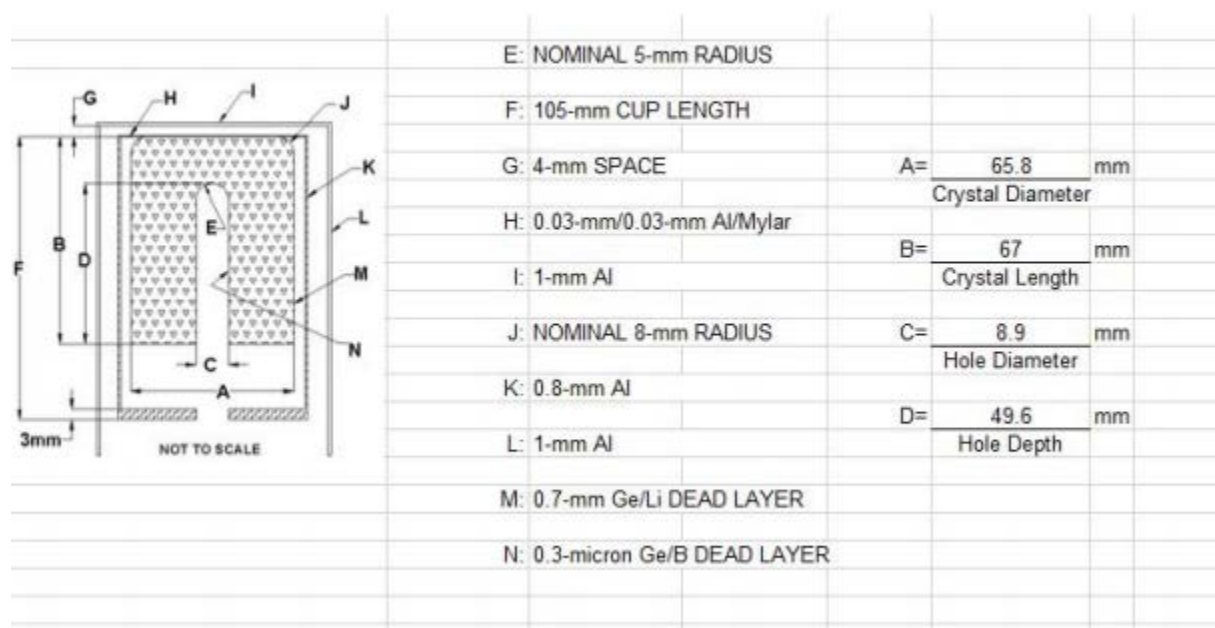


Fig. 5: Internal diagram of HPGe detector.

The slag was analyzed as soon as possible in order to look for any short half-life isotopes produced. Due to the half-life of nickel, the nickel samples were analyzed the day after irradiation, allowing the slag samples to be counted very quickly. There were also later, and longer, runs done to look for long and very long half-life isotopes.

The counting was performed by using scotch tape to affix the plastic bag containing the sample to a plastic block. The samples were attached to the plastic block in such a way as to keep them suspended directly away from, and aligned with the center of, the detector as shown in Fig. 6. The earlier runs were performed with the sample placed approximately 50 cm away from the detector face. This was the minimum distance needed to keep the dead time of the detector below 5% in order to mitigate the systematic error of the detector.

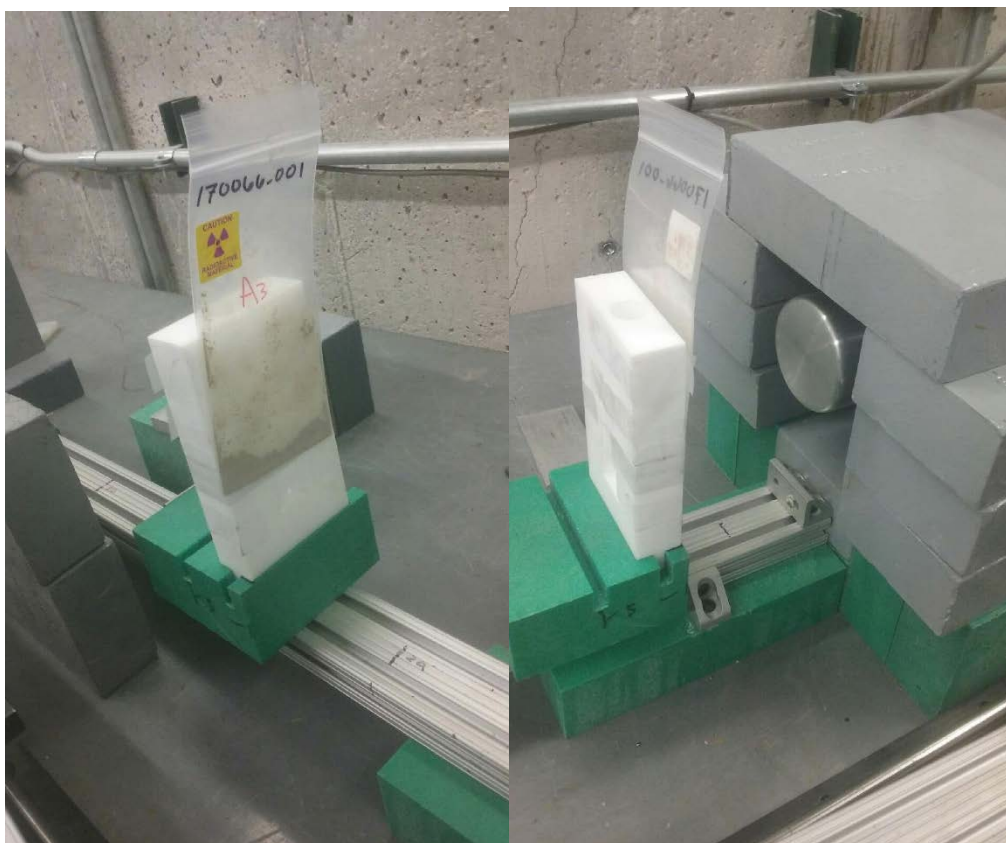


Fig. 6: Placement of the sample in front of HPGe detector for counting.

3.3 Coal, Coal Ash and Fly Ash

Coal is a complex mixture of both organic and inorganic compounds. It has a widely varying composition because it is formed from the accumulation of plant and mineral matter in a particular area and no two areas possess the exact same plant and mineral matter. This unknown composition makes the determination of the abundance of trace elements in the coal a complex task. Due to the environmental regulations surrounding the burning of coal and tracking what is released into the environment, a quick and cheap method of trace element analysis is highly beneficial.

This experiment also used PAA to determine the trace elements in samples using the same technique applied to the mining slag. However, because coal has a better characterized matrix it was possible to use a higher energy of 32 MeV, to increase the reaction rate without worrying about first order interference from undesired reactions. This experiment utilized the rare earth mixture created for the mining slag to act as an internal calibration standard for the coal, coal ash and fly ash exactly as it was used with the mining slag. Once again, nickel foil was wrapped around and Kapton taped to the outside of the vial to act as an external flux monitor. Due to beam and counting time restrictions, the number of samples was reduced from 4 to 3. Table 7 lists the samples and their specifications. The shorthand for coal is “C”, fly ash is “F”, and coal ash is “A”.

Similar to the slag, an attempt was made to get the matrix masses as close to 1 gram as possible. However, due to the very low density of the fly ash, the matrix size was reduced in order to maintain sample homogeneity. For this experiment, though there was excess fly ash to make the three 1 gram samples, it was sourced from different locations so its homogeneity could not be verified. These samples were all weighed using an identical technique to the mining slag. They were also stored in glass vials sealed with Parafilm and marked with their sample identification letter and number.

In order to maximize flux and minimize delays in counting, it was decided to irradiate each matrix type separately. On the first day, samples C1-3 were irradiated and counted that night. The next day, samples F1-3 were irradiated and counted that night. On the final day samples A1-3 were irradiated and counted that night. The samples were affixed together using Kapton tape, and placed directly in front of the bremsstrahlung converter.

After irradiation, the samples were processed by the health physicist at the Idaho Accelerator Center. This processing involved the transfer of the now radioactive matrix from the

glass vials they were irradiated in to a small plastic sealed bag. The nickel foils were once again separated into their own baggies for individual counting. Due to the higher beam energy, the nickel foils were only counted for approximately 5 minutes. Ten thousand counts and less than 1% error were obtained on the nickel 1337 keV gamma line used for the flux calibration.

After processing, the samples were still extremely radioactive. This was due to the $^{12}\text{C}(\gamma, n)^{11}\text{C}$ and $^{13}\text{C}(\gamma, nn)^{11}\text{C}$ reactions producing a large quantity of C-11. C-11 has a 20 minute half-life; so, while the samples were very hot because of that, they quickly cooled down to countable activities. The first sample counted in each case was the pure sample, because it was the least active due to not having had extra elements added. Then the two spiked samples were counted. Finally, the pure sample was counted overnight to look for long lived isotopes.

Chapter 4

Results

4.1 Slag

It was observed very early on in the analysis that a gamma line of 1157 keV quickly appeared in the sample with no spike. This energy line is associated with only two isotopes, Sc-44 and K-44. K-44 has two strong lines associated with it; the 1157 keV line with an intensity of ~59%, and another at 2150 keV with an intensity of ~23% [3,4]. However, there was no detected signal at 2150 keV, meaning the 1157 keV line must correspond to Sc-44. The Sc-44, which would have been created by the $^{45}\text{Sc}(\gamma, n)^{44}\text{Sc}$ reaction, validates the hypothesis that the slag contains appreciable amounts of scandium.

There is also an 1836 keV gamma line which can be attributed to either Y-88 or Rb-88. Rb-88 has a half-life of approximately 18 minutes, thus if this line was due to Rb-88 it would quickly die out. However, this line is strongly present in a count started over 2 hours - or more than 7 half-lives - after the end of irradiation. By comparing an early count (20 minutes after irradiation end) to this later count, it was easily shown that the activity could not be due to Rb-88. Thus the 1836 keV line can be due only to the activation of yttrium via the $^{89}\text{Y}(\gamma, n)^{88}\text{Y}$ reaction.

For cerium, the lines of interest were ones that corresponded to Ce-139 or Ce-141. A dominant gamma ray line for Ce-139 is at 165 keV, however this line was not detected in any samples. Ce-141 has a dominant line at 145 keV, but this line was also not detected in any samples. Ce-137 was not considered because its reactions have extremely low gamma intensities; the highest of these being a 34 hour half-life 254 keV line at 11% intensity. Ce-136 has approximately

0.2% natural abundance, which makes seeing any lines from Ce-135 - created by the $^{136}\text{Ce}(\gamma, n)^{135}\text{Ce}$ reaction - not feasible.

Due to the low energy used, praseodymium is not detectable. The reaction of interest is the $^{141}\text{Pr}(\gamma, n)^{140}\text{Pr}$ reaction. However, Pr-140 only has a 3.39 minute half-life and very low intensity gammas. Praseodymium has been detected using PAA before, but it relies upon photo neutron activation and 511 keV annihilation coincidence counting, which was not the focus of this experiment [1].

Europium can potentially be detected via $^{151}\text{Eu}(\gamma, n)^{150}\text{Eu}$ or $^{153}\text{Eu}(\gamma, n)^{152}\text{Eu}$. Eu-151 and Eu-153 are almost equally abundant at approximately 48% and 52% abundance, respectively, so both reactions are probable. Eu-150 has a metastable state with a 12.8 hour half-life, but the highest intensity gamma line is 333.9 keV with only a 4% intensity. Eu-152 has a 121.77 keV line with only a 7% intensity.

DATA	End of Irradiation	Start of Count	Duration of Count (s)	Dead Time	Measured Counts
Sample A	2/13/17 @ 1603	2/13/17 @ 18:21:53	8854	0.0221	841
Sample B	2/13/17 @ 1603	2/13/17 @ 21:02:10	911	0.02	1367
Sample C	2/13/17 @ 1603	2/13/17 @ 21:20:00	177	0.0237	1212
Sample D	2/13/17 @ 1603	2/13/17 @ 20:51:28	528	0.029	11781
Ni-A	2/13/17 @ 1603	2/14/17 @ 10:40:04	1534	0.0348	111662
Ni-B	2/13/17 @ 1603	2/14/17 @ 11:15:03	656	0.0177	26049
Ni-C	2/13/17 @ 1603	2/14/17 @ 11:27:31	626	0.0284	40301
Ni-D	2/13/17 @ 1603	2/14/17 @ 11:39:13	606	0.0182	23232

Table 1: Slag and nickel count data.

DATA	Initial Activities (Counts/sec)
Sample A	0.179
Sample B	3.738
Sample C	17.718
Sample D	53.881
Ni - A	108.816
Ni - B	58.854
Ni - C	96.851
Ni - D	57.289

Table 2: Slag and nickel initial activity calculation.

	Slag Masses (g)		Ni-Foils Masses (g)
Sample A	1.046	Ni - A	0.1249
Sample B	1.088	Ni - B	0.12
Sample C	1.0344	Ni - C	0.1115
Sample D	0.9942	Ni - D	0.1403

Table 3: Slag and nickel masses.

	Flux (γ /mass)
Sample A	871.22568
Sample B	490.44728
Sample C	868.62306
Sample D	408.32967

Table 4: Mass-Normalized flux.

Mixture	Mass(g)	Mass %	Mass % in Oxide	
Sc	0.3498	0.248	0.652	
Ce	0.2495	0.177	0.814	
Pr	0.256	0.182	0.828	
Y	0.2389	0.170	0.787	
Eu	0.3137	0.223	0.864	
Total	1.4079			
	Mixture Amount Added (mg)			Sc Added (mg)
Sample A	0		Sample A	0
Sample B	3.5		Sample B	0.57
Sample C	12.7		Sample C	2.06
Sample D	70.6		Sample D	11.0

Table 5: Scandium in spike mixture.

	Micrograms of Sc/Gram of Slag	Micrograms of Y/Gram of Slag
Sample A/B	15.03	253.36
Sample A/C	20.01	N/a
Sample A/D	17.05	257.10
Average	17.4 ± 2.0	255.2 ± 1.9

Table 6: Concentration of scandium and yttrium in slag.

4.2 Coal, Coal Ash and Fly Ash

When analyzing the coal sample data, the only gamma peak corresponding to the rare earth elements found was the Sc-44 line at 1157 keV. This does not mean that there are no other rare earth elements in the coal, simply that if they are there, they are below the detectable limit. However, because the coal ash and fly ash are more concentrated, it was still possible to detect these elements in them.

Further analysis of the coal ash and fly ash also revealed the line at 1157 keV, which meant they also contained scandium. Thus the scandium is deposited in the by-products and is not entirely volatilized. No additional rare earth elements were detected in the coal ash, however a very small signal measured at 1836 keV meant that yttrium was detected in the fly ash. The data for the coal samples is listed in tables 8-12, the data for the coal ash samples is listed in tables 13-16, and the data for the fly ash samples is listed in tables 17-20.

Sample	Matrix Mass (g)	Spike Mass (mg)	Foil Mass (g)
C1	1.0483	0	0.115
C2	1.0644	3.8	0.1086
C3	1.0851	69.9	0.1014
F1	1.063	0	0.0969
F2	1.0748	6.1	0.0963
F3	1.0522	67.5	0.097
A1	0.3909	0	0.1005
A2	0.4164	5	0.094
A3	0.3844	66.1	0.0966

Table 7: Masses of samples, spikes and Ni-foils.

Sc Runs	Start Time/Date	Live Time	Counts	%Error	%Dead Time
Sample C1	5/23/2017 22:52:01	28885	908	6.26	0.25
Sample C2	N/a	N/a	N/a	N/a	N/a
Sample C3	5/24/2017 6:56:38	1372	26928	0.61	2.80
Ni - C1	5/23/2017 16:37:00	294	14125	0.85	2.27
Ni - C2	5/23/2017 16:45:58	454	16696	0.78	1.93
Ni - C3	5/23/2017 16:54:27	447	12655	0.89	1.43

Table 8: Coal count data.

	Coal Masses (g)	Ni-Foils Masses (g)
Sample C1	1.0483	0.115
Sample C2	1.0644	0.1086
Sample C3	1.0851	0.1014

Table 9: Coal and Ni-foil mass data.

Mixture	Mass(g)	Mass %	Mass% in Oxide
Sc	0.3498	0.248	0.652
Ce	0.2495	0.177	0.814
Pr	0.256	0.182	0.828
Y	0.2389	0.170	0.787
Eu	0.3137	0.223	0.864

Table 10: Rare earth element mixture data.

	Mixture Added (mg)	Sc Added (mg)
Sample C1	0	0
Sample C2	3.8	0.62
Sample C3	69.9	11.3

Table 11: Mixture and scandium added to coal data.

	$\mu\text{g Sc/g Coal}$
Sample C1/C2	N/a
Sample C1/C3	4.94
Average	4.9 ± 0.1

Table 12: Calculated scandium concentration in coal.

Sc Runs (1157keV)	Start Time/Date	Live Time	Counts	%Error	%Dead Time
Sample A1	5/24/2017 17:09:47	1251	973	4.5	5.07
Sample A2	5/24/2017 17:35:52	572	13334	0.88	5.16
Sample A3	5/24/2017 17:51:32	226	12506	0.9	5.57
A1-2754	5/24/2017 17:09:47	1251	11422	0.94	5.07
A2-2754	5/24/2017 17:35:52	572	3328	1.74	5.16
A3-2754	5/24/2017 17:51:32	226	222	7.06	5.57
Y Runs (898keV)	Start Time/Date	Live Time	Counts	%Error	%Dead Time
Sample A1	5/24/2017 17:09:47	1251	44	39.22	5.07
Sample A2	5/24/2017 17:35:52	572	189	17.72	5.16
Sample A3	5/24/2017 17:51:32	226	206	14.49	5.57
A1-2754	5/24/2017 17:09:47	1251	11422	0.94	5.07
A2-2754	5/24/2017 17:35:52	572	3328	1.74	5.16
A3-2754	5/24/2017 17:51:32	226	222	7.06	5.57

Table 13: Scandium and yttrium in coal ash count data.

	Coal Ash Masses (g)	Ni-Foils Masses (g)
Sample A1	0.3909	0.1005
Sample A2	0.4164	0.094
Sample A3	0.3844	0.0966

Table 14: Coal ash and Ni-foil mass data.

	Mixture Added (mg)	Sc Added (mg)	Y Added (mg)
Sample A1	0	0	0
Sample A2	5.0	0.81	0.67
Sample A3	66.1	10.7	8.83

Table 15: Mixture, scandium and yttrium added data.

	$\mu\text{g Sc}/(\text{g of Coal Ash})$	$\mu\text{g Y}/(\text{g of Coal Ash})$
Sample A1/A2	46.15	136.62
Sample A1/A3	40.20	100.57
Average	43.2 ± 3.0	118.6 ± 18.0

Table 16: Calculated scandium and yttrium concentration in coal ash data.

Sc Runs (1157keV)	Start Time/Date	Live Time	Counts	%Error	%Dead Time
Sample F1	5/24/2017 18:01:20	47220	7610	1.7	0.89
Sample F2	5/24/2017 17:17:43	2224	10267	1.01	1.83
Sample F3	5/24/2017 17:56:04	238	15406	0.81	7.71
Ni - F1	5/24/2017 16:42:35	172	17755	0.76	5.22
Ni - F2	5/24/2017 16:46:22	205	12606	0.9	3.03
Ni - F3	5/24/2017 16:50:28	185	16730	0.78	4.40
Y Runs (898keV)	Start Time/Date	Live Time	Counts	%Error	%Dead Time
Sample F1	5/24/2017 18:01:20	47220	276	18.99	0.89
Sample F2	5/24/2017 17:17:43	2224	104	14.79	1.83
Sample F3	5/24/2017 17:56:04	238	157	8.75	7.71
Ni - F1	5/24/2017 16:42:35	172	17755	0.76	5.22
Ni - F2	5/24/2017 16:46:22	205	12606	0.9	3.03
Ni - F3	5/24/2017 16:50:28	185	16730	0.78	4.40

Table 17: Scandium and yttrium in fly ash count data.

	Fly Ash Masses (g)	Ni-Foils Masses (g)
Sample F1	1.063	0.0969
Sample F2	1.0748	0.0963
Sample F3	1.0522	0.097

Table 18: Fly ash and Ni-foil mass data.

	Mixture Added (mg)	Sc Added (mg)	Y Added (mg)
Sample F1	0	0	0
Sample F2	6.1	0.99	0.82
Sample F3	67.5	10.9	9.02

Table 19: Mixture, scandium and yttrium added data.

	$\mu\text{g Sc}/(\text{g of Fly Ash})$	$\mu\text{g Y}/(\text{g of Fly Ash})$
Sample F1/F2	54.79	60.23
Sample F1/F3	53.64	61.44
Average	54.2 ± 0.6	60.8 ± 0.6

Table 20: Calculated scandium and yttrium concentration in fly ash data.

4.3 Mathematical Analysis Derivation of Ratio Method

It can be easily understood that the activity of the gamma line in question is directly proportional to the amount of the isotope that created that line. The amount of the isotope is then also directly proportional to the original element that was irradiated to become that isotope. Therefore, it can be stated that the activity of the gamma line is proportional to the quantity of element being investigated. This starting point is called Baseline 1.1.

$$\text{Activity of Sample} \propto \text{Total Amount of Element in Sample} \quad \text{Baseline 1.1}$$

$$A(\text{Sample}) \propto E(\text{Sample}) \quad \text{Baseline 1.2}$$

However, the activity of the samples is always changing due to the decay of the isotopes. This means that the activities of the samples must all be compared at some shared time. For the purposes of this analysis the time used was the end of irradiation. Thus there is a need to back

calculate some initial activity which corresponds to the activity of the gamma line in question at the end of irradiation. Starting from the standard exponential decay equation (Eqn.) 1.1:

$$A = A_0 * e^{-\lambda t} \quad (1.1)$$

$$\int_{t_1}^{t_2} A * dt = \int_{t_1}^{t_2} A_0 * e^{-\lambda t} * dt \quad (1.2)$$

$$True Counts = \frac{-A_0}{\lambda} * (e^{-\lambda t_2} - e^{-\lambda t_1}) \quad (1.3)$$

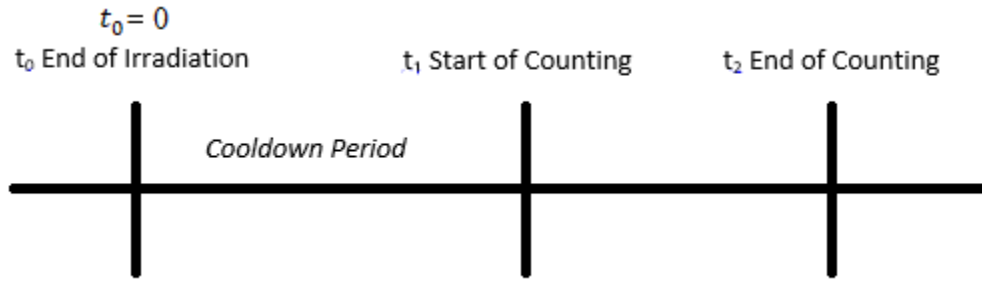


Fig. 7: Timeline for irradiation and counting.

In Eqns. 1.2 and 1.3, t_1 is the amount of time from the end of irradiation to the start of counting and t_2 is the time from the end of irradiation to the end of counting as shown in Fig. 7. The activity at any specific point in time is not known, so Eqn. 1.1 is integrated from t_1 to t_2 to turn activity into counts. However, detectors can miss counts due to the buildup of more signals than they can measure within a certain time frame, thus detectors do not give true counts. This phenomenon is known as dead time and MPA calculates it by default. So, in order to get the true counts a perfect detector would register, the measured counts must be increased to the true counts value by dividing by the average percentage of live time; this adjustment is shown in Eqn. 2.1.

$$True Counts = \frac{Measured Counts}{Live Time Fraction} = \frac{Measure Counts}{1 - Dead Time Fraction} = \frac{C}{1 - D} \quad (2.1)$$

$$\frac{C}{1 - D} = \frac{-A_0}{\lambda} * (e^{-\lambda t_2} - e^{-\lambda t_1}) \quad (2.2)$$

$$A_0 = \frac{C * \lambda}{(e^{-\lambda t_1} - e^{-\lambda t_2}) * (1 - D)} \quad (2.3)$$

Substituting the value for true counts calculated in Eqn. 2.1 into 1.3 yields Eqn. 2.2, which is then solved for the only unknown, A_0 . In Eqn. 2.3. C is the counts measured by the MPA program; D is the dead time given by the program in decimal form; and λ is the decay constant of the isotope responsible for the gamma line being investigated.

The initial activity equation can now be used to calculate the initial activity of our samples and relate it to the quantity of the element in the sample. However, not all samples received the same flux, thus the initial activity must be scaled by the amount of flux received. To this end Eqn. 3.1 is combined with Baseline 1.2 turning them into Eqn. 3.2. The flux received is proportional to the activity of the nickel foils divided by the mass of the nickel foils as shown in Eqn. 3.1. The activities of the nickel foils also need to be back calculated to some initial activity using Eqn. 2.3.

$$Flux(Sample) \propto \frac{A_0(Nickel)}{Mass\ of\ Nickel} \quad (3.1)$$

$$\frac{A_0(Sample)}{Flux(Sample)} \propto \frac{A_0(Sample)}{\frac{A_0(Nickel)}{Mass\ of\ Nickel}} \propto E(Sample) \quad (3.2)$$

Since it is more useful to talk about concentrations rather than absolute amounts, Eqn. 3.2 can be slightly modified by introducing x , where x has units of micrograms of element per gram of matrix. Introducing this requires a modification of the right hand side of Eqn. 3.2, as shown in Eqn. 4.1.

$$E(Sample) = x * Mass\ of\ Sample \frac{w}{o} Spike + Amount\ of\ Element\ Added\ By\ Mixture \quad (4.1)$$

$$E(Sample) = x * M(Sample) + add(Sample) \quad (4.2)$$

By combining Eqn. 4.2 and 3.2, Eqn. 5.1 is obtained. Finally, take the ratio of Eqn. 5.1 for two different samples; the constant of proportionality divides out making the ratio equal instead of proportional, which yields Eqn. 5.2. Since sample A is not spiked, the added value is 0, $add(a) = 0$, and has been removed. Solving 5.2 for the unknown concentration x yields Eqn. 5.3.

$$\frac{A_0(Sample)}{Flux(Sample)} \propto x * M(Sample) + add(Sample) \quad (5.1)$$

$$\frac{A_0(a)}{Flux(a)} \div \frac{A_0(b)}{Flux(b)} = \frac{x*M(a)}{x*M(b)+add(b)} \quad (5.2)$$

$$x = \frac{A_0(a)*add(b)*Flux(b)}{A_0(b)*Flux(a)*M(a)-A_0(a)*Flux(b)*M(b)} \quad (5.3)$$

These equations can now be applied to our analysis of the concentration of scandium in the slag matrix. First, start with Eqn. 2.3 to calculate all of the initial activities. For this calculation the variables needed are the times of: end of irradiation, start of count, and duration of count. In addition to those are the dead time and the measured counts given by MPA. These values have been listed in Table 1. Since we are looking at Sc-44, which has a half-life of 3.97 hours, λ , which has a value of $\ln(2)$ divided by the half-life, equals $4.85E-5 \text{ s}^{-1}$. For the nickel, the interesting isotope is Ni-57, which has a half-life of 35.6 hours; so for Ni-57, λ is equal to $5.41E-6 \text{ s}^{-1}$.

4.3.1 Example Calculation for Scandium in Sample A

The decay corrected initial activity is given by:

$$A_0 = \frac{C*\lambda}{(e^{-\lambda t_1}-e^{-\lambda t_2})*(1-D)} \quad (2.3)$$

Where:

$$t_1(a) = (2 \text{ hr} * 60 \frac{\text{min}}{\text{hr}} + 18 \text{ min}) * 60 \frac{\text{sec}}{\text{min}} + 53 \text{ sec} = 8333 \text{ sec}$$

$$t_2(a) = (2 \text{ hr} * 60 \frac{\text{min}}{\text{hr}} + 18 \text{ min}) * 60 \frac{\text{sec}}{\text{min}} + 53 \text{ sec} + 8854 \text{ sec} = 17187 \text{ sec}$$

$$A_0(\text{Sample A}) = \frac{(841 \text{ Counts}) * (4.85E - 5 \frac{1}{\text{sec}})}{(e^{-(4.85E-5 \frac{1}{\text{sec}})*(8333 \text{ sec})} - e^{-(4.85E-5 \frac{1}{\text{sec}})*(17187 \text{ sec})}) * (1 - 0.0221)}$$

$$A_0(a) = 0.17897 \frac{\text{Counts}}{\text{sec}}$$

Performing the same calculation for the other samples and the nickel foils gives the results in table 2. Next Eqn. 3.1 is used to solve for the relative flux that each sample received. This is accomplished by using the initial activities listed in table 2 and the masses of the nickel foils listed in table 3 along with the slag masses.

To finally solve Eqn. 5.3, all that is needed are the amounts of scandium added to each sample. Since the mixture used to spike the samples was homogeneously mixed, the amount of element added is equal to the percent of element present in the mixture. However, the elements exist in an oxide state, so the percent mass in the oxide must also be considered. This calculation is shown in Eqn. 6.1.

Sc Added to Sample =

$$\text{Mass of Spike Added} * \frac{\text{Mass of Element Oxide}}{\text{Mass of Spike Added}} * \frac{\text{Mass of Element}}{\text{Mass of Element Oxide}} \quad (6.1)$$

Table 5 lists the amount of mixture added to each sample as well as the composition of the mixture. It also contains the values for the percentage mass in the mixture, which was simply calculated as the amount of scandium in the mixture divided by the total mass of the mixture, as well as the percentage of mass of scandium in scandium oxide.

Eqn. 6.1 Calculated for Sample B

$$add(b) = 3.5mg \text{ Mixture} * \frac{0.3498 \text{ Sc Oxide}}{1.4079 \text{ g Mixture}} * 0.65196 \frac{Sc}{Sc \text{ Oxide}} = 0.56694 \text{ mg Sc}$$

Eqn. 5.3 Calculated for Sample A/Sample B

$$x = \frac{A_0(a) * add(b) * Flux(b)}{A_0(b) * Flux(a) * M(a) - A_0(a) * Flux(b) * M(b)}$$

$$= \frac{0.17897 \frac{Counts}{sec} * 566.94 \mu g \text{ Sc} * 490.44728}{3.73818 \frac{Counts}{sec} * 871.22568 * 1.046 \text{ g Slag} - 0.17897 \frac{Counts}{sec} * 490.44728 * 1.088 \text{ g Slag}}$$

$$= 15.0 \frac{\mu g \text{ Sc}}{g \text{ Slag}}$$

This calculation was then repeated with the values for Sample B replaced with the values for Sample C, and finally with the values for Sample D. Samples B, C, and D are all compared to A to minimize measurement error. The concentrations are then averaged together to create a value of 17.36 micrograms of scandium per gram of slag. The value for each calculation and the average are listed in Table 6. This exact process was duplicated for the yttrium line, and its values are also listed in Table 6.

4.4 Extrapolation Method

During the investigation of the ratio method results there was a very large discrepancy between the two concentration values for yttrium in coal ash. The other values from all the samples agreed within $\pm 10\%$ of the average value, except for the yttrium in coal ash which had a margin of error of approximately $\pm 100\%$. It was believed that there may be a flaw in the ratio method, thus it was decided to verify the values using a different method.

The basis of this method is that the activity of a gamma line from a sample is directly proportional to the amount of element creating that line in the sample. Therefore if the activity is plotted on the y-axis and amount of element in the sample is plotted on the x-axis there will be a linear relationship. The amount of element in the sample is unknown so the amount of element added is used instead.

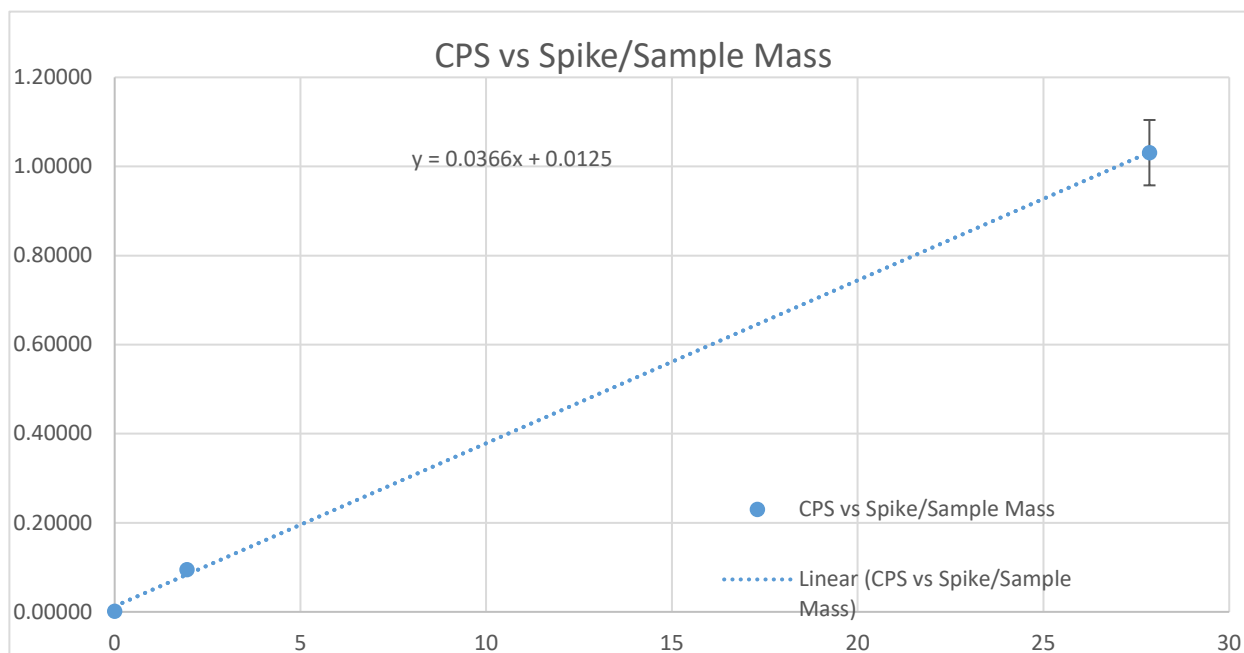
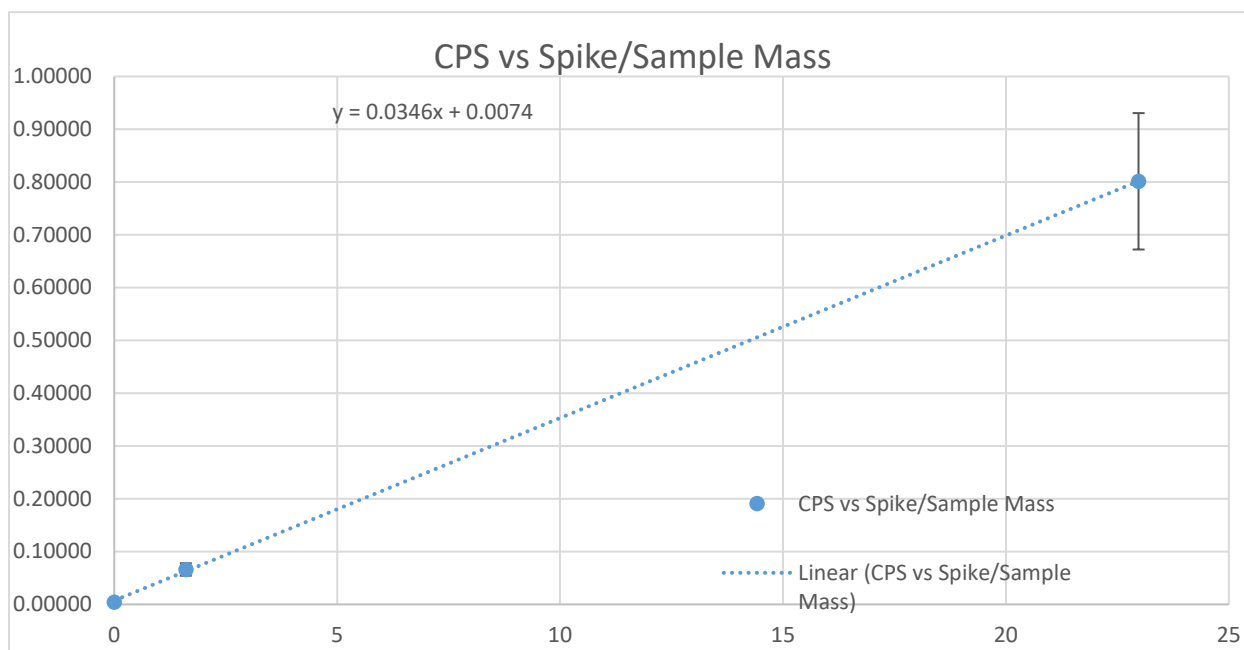
The value of interest is where this line crosses the x-axis. If the line crosses at x equals zero then it can be interpreted that there is no intrinsic concentration of element in the sample since its activity at zero element added is zero. If instead it crosses at some negative value of x there is some measurable intrinsic concentration of element in the sample. This value is found by extrapolating the best fit line to where activity is equal to zero. The negative x value is the concentration of element which would have to be removed from the sample in order to reduce its activity at the line of interest to zero. Stated in another way, the magnitude of that negative x value is equal to the intrinsic concentration of the element in the sample.

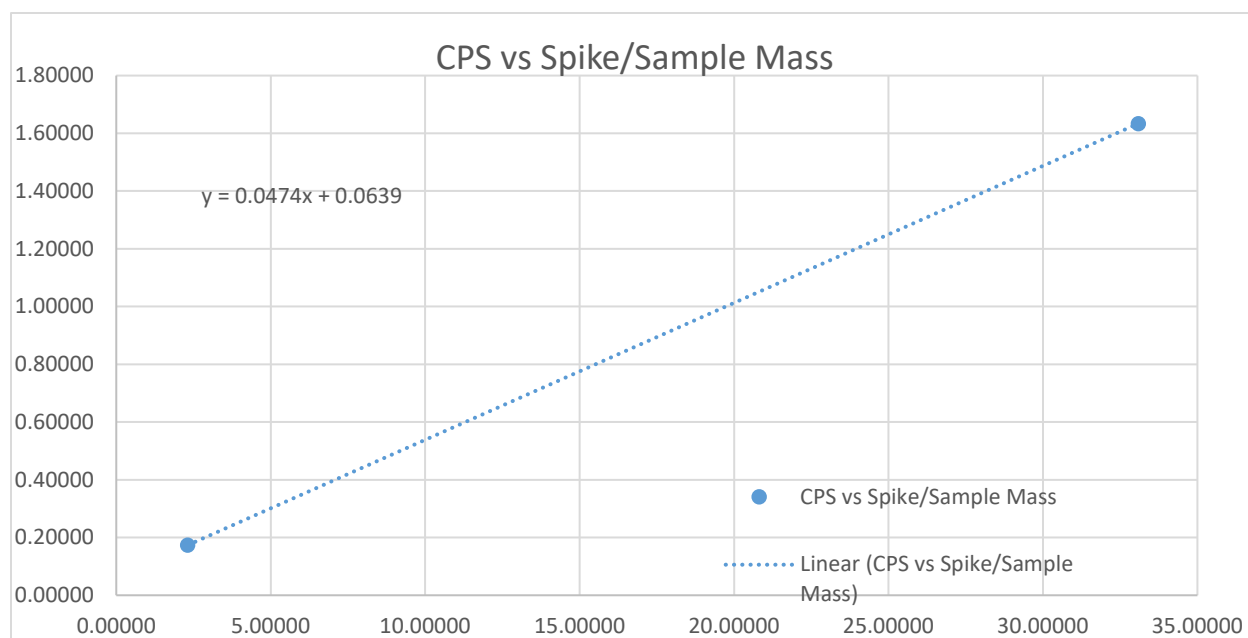
While performing the extrapolation method the results did not form a linear relationship. This lack of linear relationship was due to an error in the nickel foil activity data. This error could have arisen from a discrepancy of the labels during counting. It could have also been caused by the foil receiving much more flux than the sample due to the experimental setup. This error was rectified by using an internal flux monitor instead of the external nickel foil flux monitor. In looking for an internal flux monitor several lines appeared to be of use. These were all compared and the one with values closest to the average was used. The ratios of the values of all the internal lines are listed in Table 21 and are contrasted with the faulty nickel line ratios.

Coal Ash	A2/A1	A3/A1
Na-24		
1368 keV	0.60015	0.12632
2754 keV	0.60515	0.11189
K-43		
372.8 keV	0.62652	0.18288
617.8 keV	0.58345	0.12004
Sr-87		
388.8 keV	0.60892	0.14265
Average	0.60484	0.13676
Ni-57	Ni-2/Ni-1	Ni-3/Ni-1
1377 keV	0.64760	0.69331

Table 21: Summary of internal line and nickel ratios.

As seen in Table 21 the ratios between the internal lines of samples 2 and 1 are very similar to the nickel ratios and the ratios between 3 and 1 are very different. The 2754 keV line of Na-24 has values that are closest to the average, therefore it was chosen to be the line used as the internal flux monitor. Once the analysis was performed while swapping all of the nickel values for the Na-24 values, the best fit line made a much closer linear fit as expected for the yttrium and europium in coal ash. A verification analysis was also performed on scandium in coal ash and was found to agree within ten percent of the average with the ratios method. The graphs of the best fit lines are found in Figs. 8-10, and the best fit lines were produced using the python code in Appendix A. The values for the extrapolated concentrations are found in Table 22.

Fig. 8: Scandium in coal ash (counts per sec/(g* γ) vs g of mass).Fig. 9: Yttrium in coal ash (counts per sec/(g* γ) vs g of mass).

Fig. 10: Europium in coal ash (counts per sec/(g* γ) vs g of mass).

Extrapolation Method	$\mu\text{g Sc}/(\text{g of Coal Ash})$	$\mu\text{g Y}/(\text{g of Coal Ash})$	$\mu\text{g Eu}/(\text{g of Coal Ash})$
Coal Ash	39.40	107.18	1348.10
Errors	± 2.56	± 55.83	± 346.31

Table 22: Calculated concentration values of Sc, Y and Eu in coal ash.

Using an internal flux monitor can be a superior alternative to using an external flux monitor. An internal flux monitor will give more accurate results than an external flux monitor, since it is directly incorporated with the sample. Because the internal monitor is inside of the sample it experiences matrix effects in an identical manner to the elements of interest. When using an internal monitor the amount of parts that need to be weighed are decreased, thereby reducing measurement error. It also eliminates the possibility of a foil getting mislabeled during either sample preparation or post irradiation processing.

4.5 Mathematical Derivation of Extrapolation Method

We use Eqn. 2.3 to calculate the initial activities of the internal flux line and the line for the element of interest, in a similar manner to the ratio method.

$$A_0 = \frac{C * \lambda}{(e^{-\lambda t_1} - e^{-\lambda t_2}) * (1 - D)} \quad (2.3)$$

Eqn. 2.3 states that the initial activity of the line (A_0) is equal to the detector measured total counts from t_1 to t_2 for the line (C) times the decay constant of the isotope that created the line (λ). This is then divided by the difference of two exponential decays with times t_1 (seconds from end of irradiation to start of counting) and t_2 (seconds from end of irradiation to end of counting). The last quantity in the equation is a factor to correct for the live time of the detector ($1 - D$), which is one minus the dead time of the detector as a decimal.

Once Eqn. 2.3 has been applied to calculate the initial activities of the flux monitor and the element, the flux monitor activity is then divided by the mass of flux monitor in the sample. This quantity is unknown, so instead it is divided by the mass of the non-spiked sample, which is proportional to the mass of the flux monitor. This new ratio (shown in Eqn. 7.1) is now proportional to the mass-normalized flux the sample received.

$$Mass_Normalized\ Flux = \frac{A_0}{mass(Sample\ w/\ no\ spike)} \quad (7.1)$$

Next, all of the element initial activities need to be normalized by the relative flux they received. This is done by dividing the initial activity of the element in a sample by the flux of the corresponding sample. This value is then used as the y-values of the mass extrapolation graph.

$$Mass_and_Flux_Normalized\ A_0 = \frac{A_0}{Flux} = y\left[\frac{cps}{g * \gamma}\right] \quad (7.2)$$

The x-values of the graph need to represent the amount of relative spike added to the sample. Using equation 6.1 from the slag derivation, we can calculate the mass of spike added.

This added spike mass is then normalized by dividing the spike mass by the total sample mass (spike plus base masses) in Eqn. 7.2.

Mass of Element Added =

$$\text{Mass of Spike Added} * \frac{\text{Mass of Element Oxide}}{\text{Mass of Spike Added}} * \frac{\text{Mass of Element}}{\text{Mass of Element Oxide}} \quad (6.1)$$

$$\text{Mass} - \text{Normalized Mass of Spike} = \frac{\text{Mass of Element Added}}{\text{Mass(Total sample)}} = x \left[\frac{\text{mg}}{\text{g}} \right] \quad (7.2)$$

When plotted against each other, these values create a line of the form $y=mx+b$. If we set our activity (y) to be zero, - just as in Eqn. 7.3 - we can solve this for an extrapolated concentration of element (x_0), which would need to be removed in order to reduce the initial activity to zero. This concentration of element which would need to be removed is equal to the baseline concentration of the element in the sample. As shown by Eqn. 7.4, this x_0 has units of mg of element per gram of sample.

$$0 = mx_0 + b \quad (7.3)$$

$$x_0 = \text{extrapolated concentration} = \text{abs}\left(\frac{b}{m}\right) \left[\frac{\frac{\text{cps}}{\text{g}*\gamma}}{\frac{\text{cps}}{\text{g}*\gamma}} \right] = \text{abs}\left(\frac{b}{m}\right) \left[\frac{\text{mg}}{\text{g}} \right] \quad (7.4)$$

Then the absolute value of the extrapolated mass is taken due the value of interest being the magnitude of the concentration from zero. Finally, the extrapolated mass is multiplied by 1000 $\mu\text{g}/\text{mg}$ in Eqn. 7.5 to turn it into an extrapolated concentration with units of microgram of element per gram of sample - also known as parts per million (ppm).

$$\text{Extrapolated concentration} = \frac{b}{m} \left[\frac{\text{mg}}{\text{g}} \right] * 1000 \frac{\mu\text{g}}{\text{mg}} = \left[\frac{\mu\text{g of element}}{\text{g of sample}} \right] \quad (7.5)$$

4.6 Missing Elements

Some of the rare earth elements Dr. Dale believed he saw in his initial runs, that this thesis is building on, were not seen. As shown in Fig. 11, Dr. Dale believed he saw La-140, which would have been created by the (γ, np) reaction on Ce-142. Figs. 12-15 show that in the samples spiked with cerium (samples B-D), there is no signal at 1596 keV. Fig. 16 shows the suspected europium signal in coal ash at 963 keV, despite that Figs. 17-20 fail to show any signals in the pure samples. Unlike the slag, the signals were seen in the spiked coal ash samples A2 and A3. In Fig. 21, there are two lines which seem to indicate the presence of yttrium in coal ash. Figs. 22-25, focus on the 898 keV line (since it has a higher branching ratio) and show that in the spiked samples the 898 keV line is visible, but the pure sample has an extremely faint reading. Fig. 26, shows a signal believed to be consistent with cerium in the fly ash sample. Figs. 27-30 show only a faint reading in the sample with the largest spike (F3).

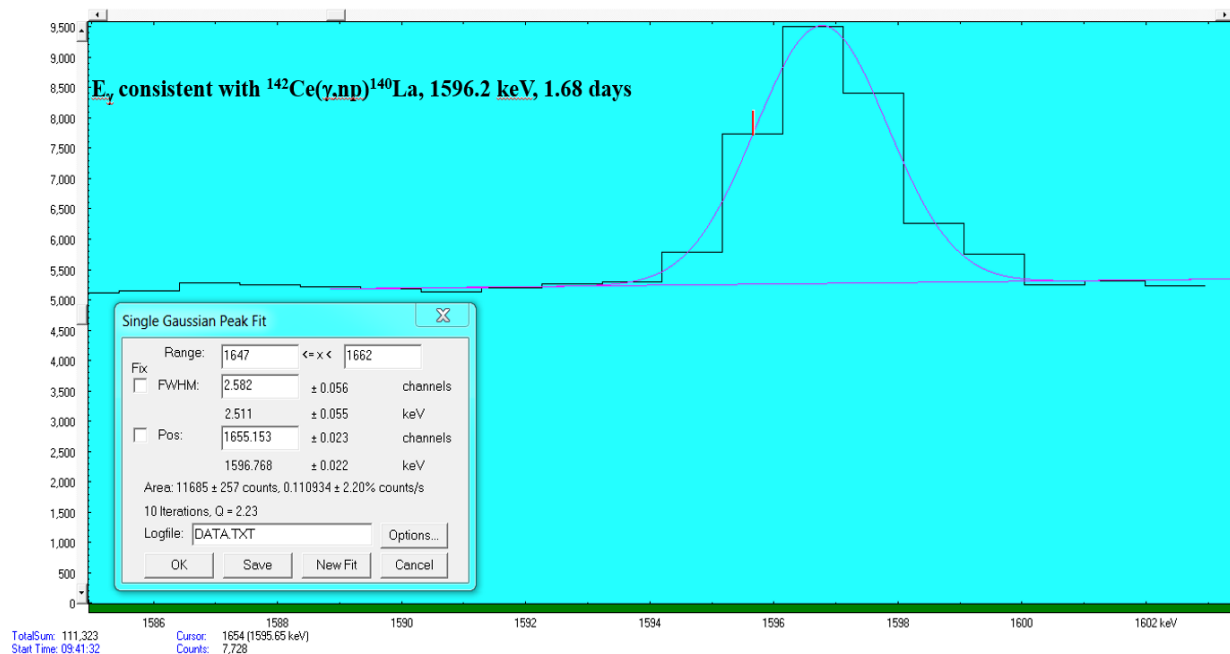


Fig. 11: Dr. Dale's Run FMC slag run 18.

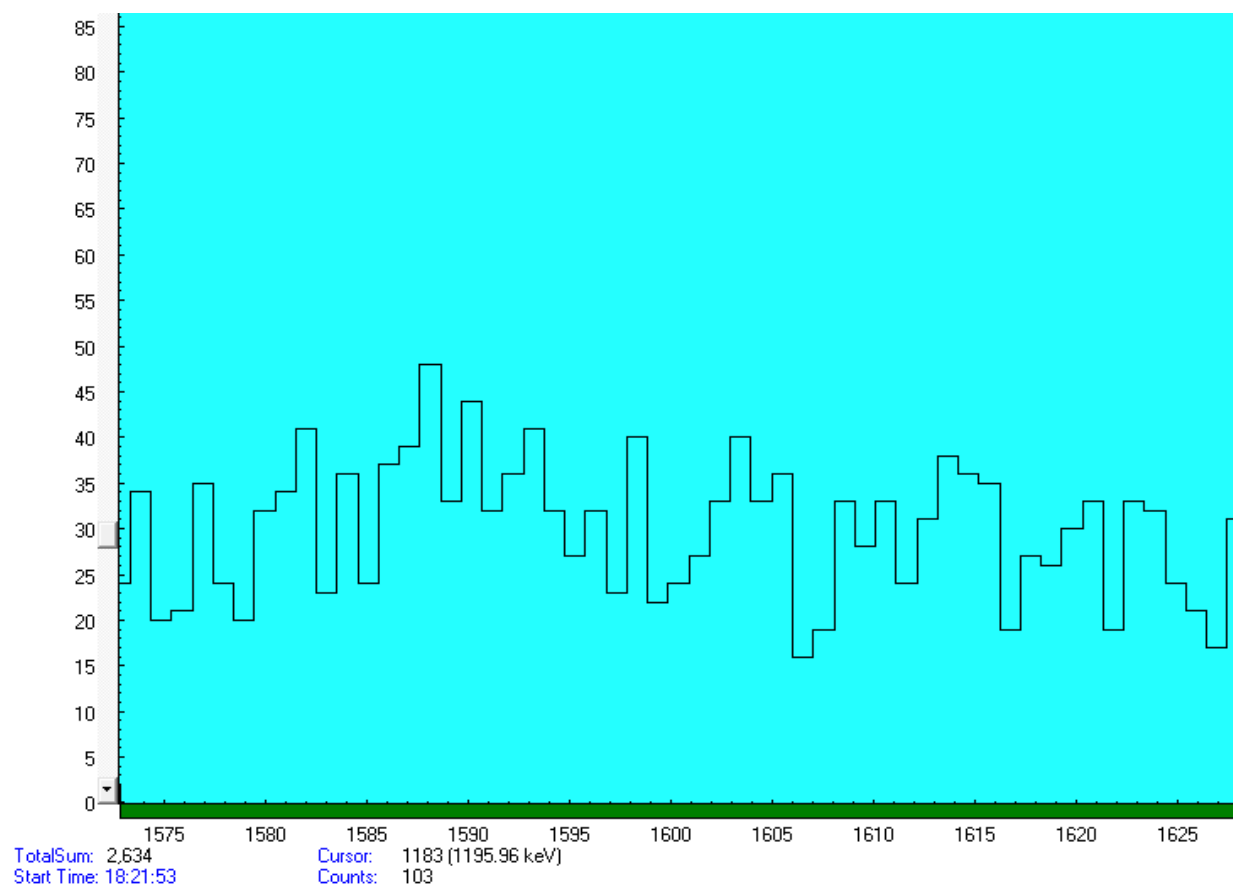


Fig. 12: Slag A, 2 Hours after beam off, 8854s count time; no 1596 keV signal.

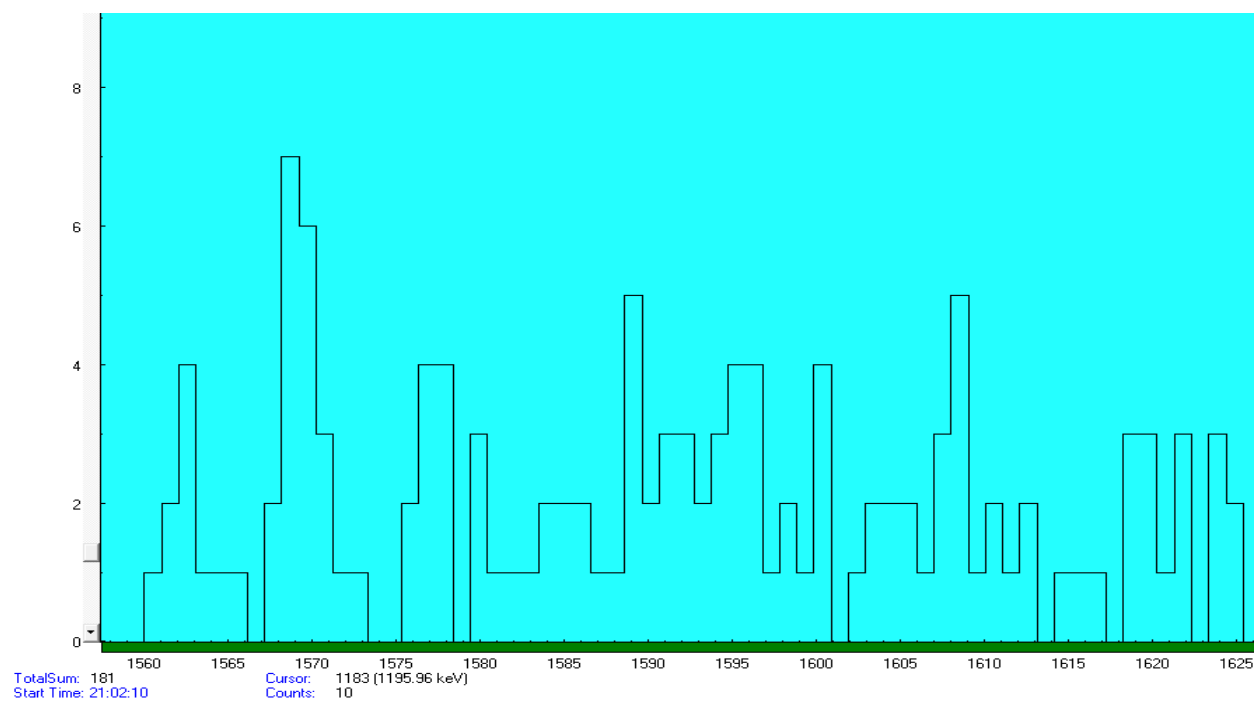


Fig. 13: Slag B, 5 hours after beam off, 911s count time; no 1596 keV signal.

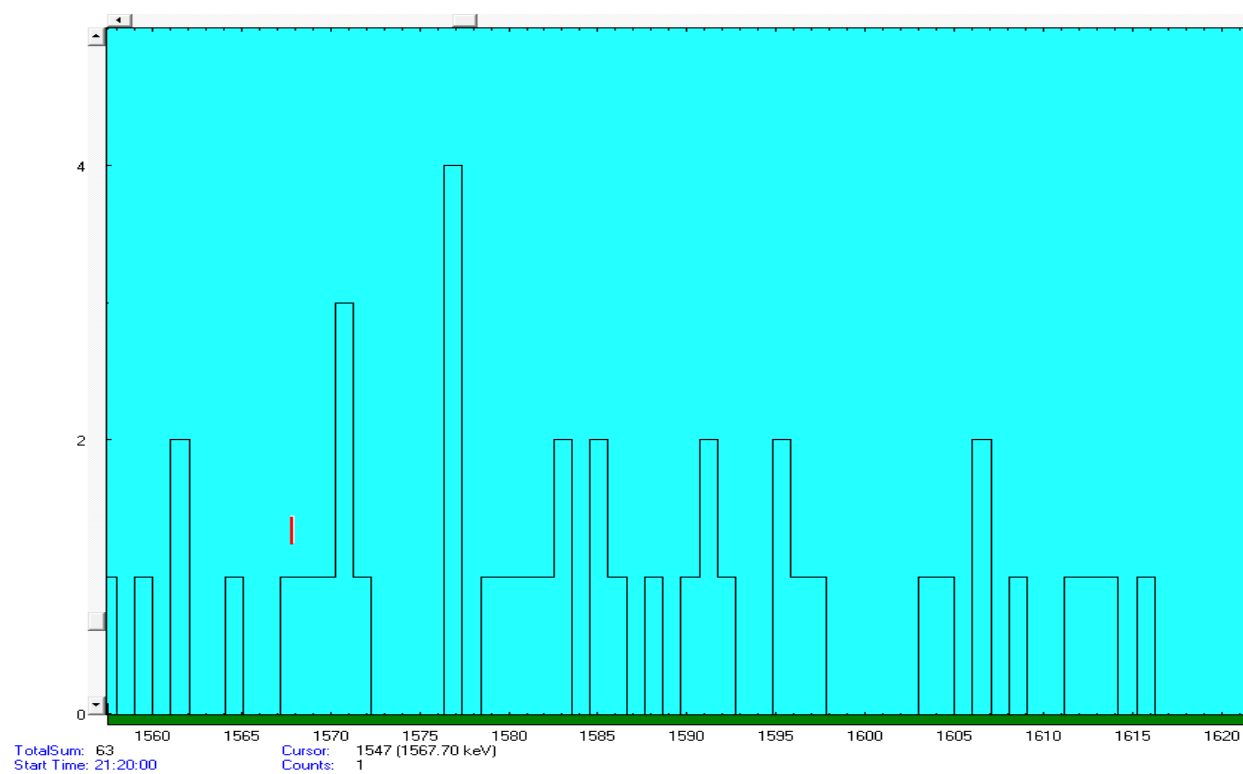


Fig. 14: Slag C, 5 hours after beam off, 177s count time; no 1596 keV signal.

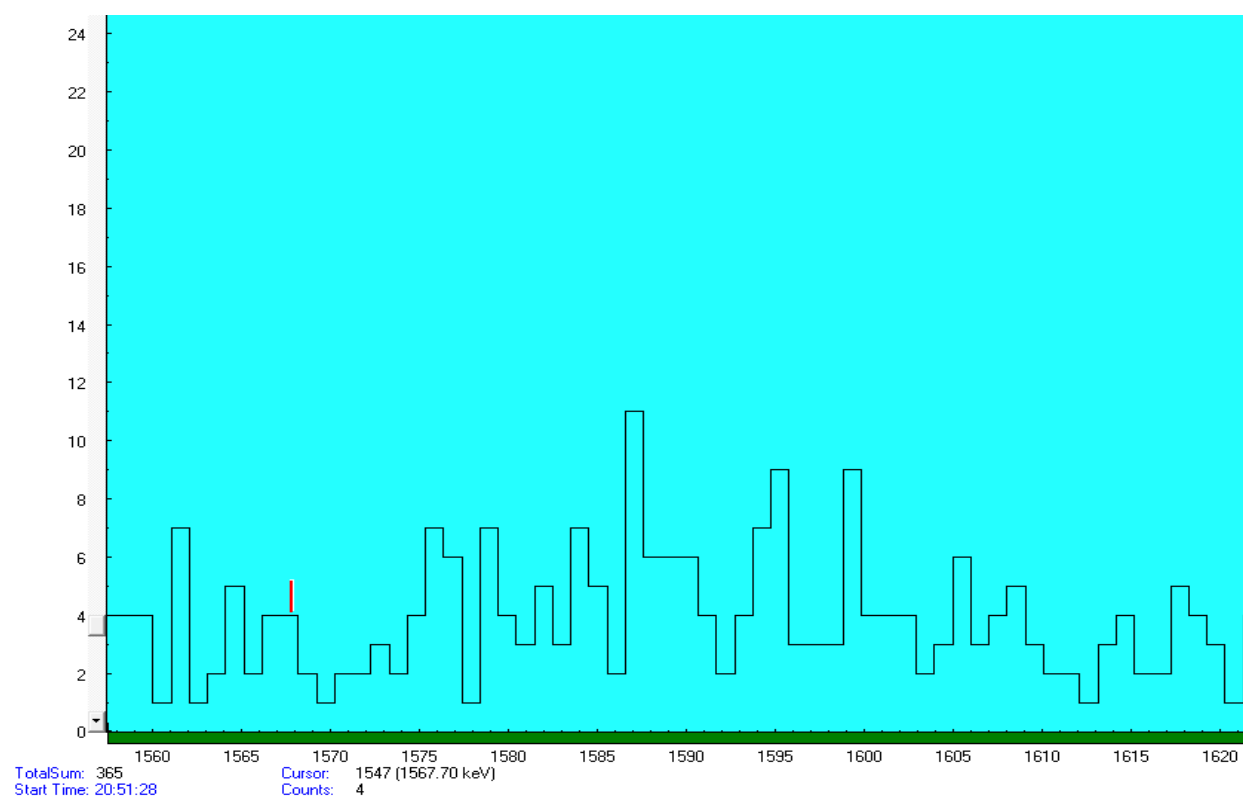


Fig. 15: Slag D, 5 hours after beam off, 528s count time; no 1596 keV signal.

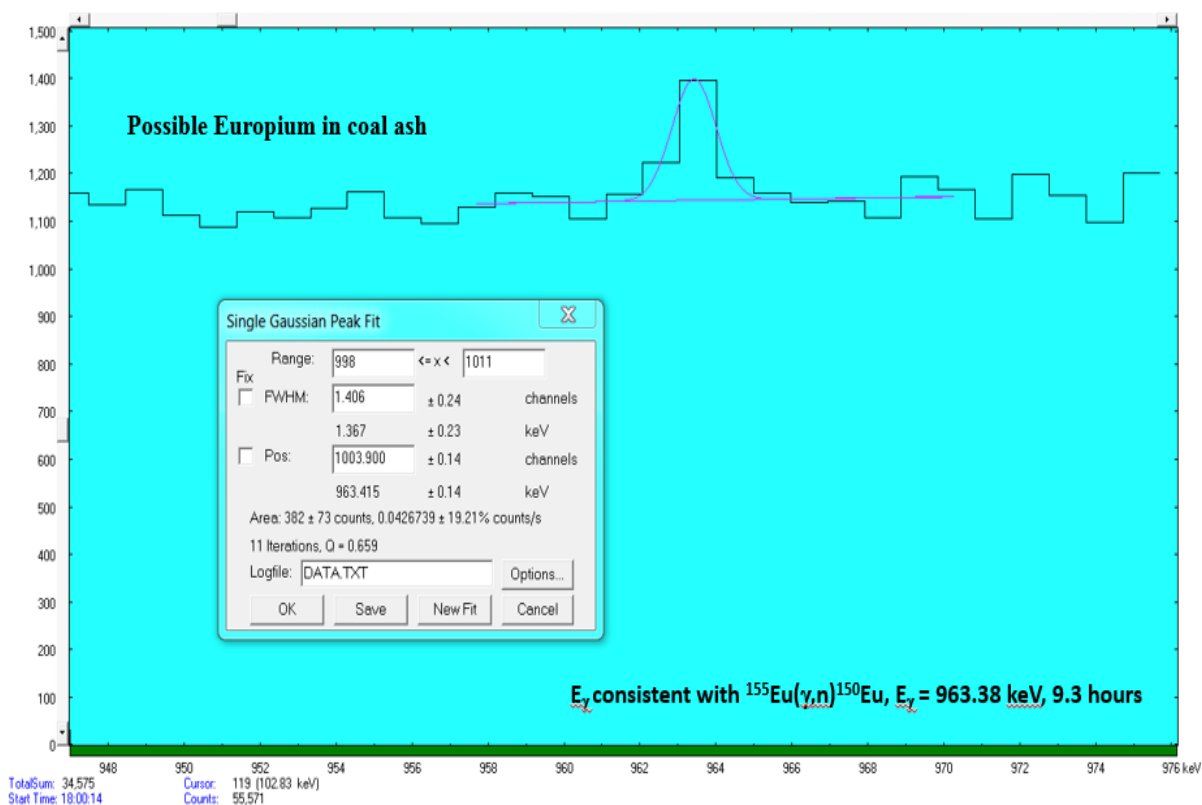


Fig. 16: Dr. Dale's coal ash run 12.

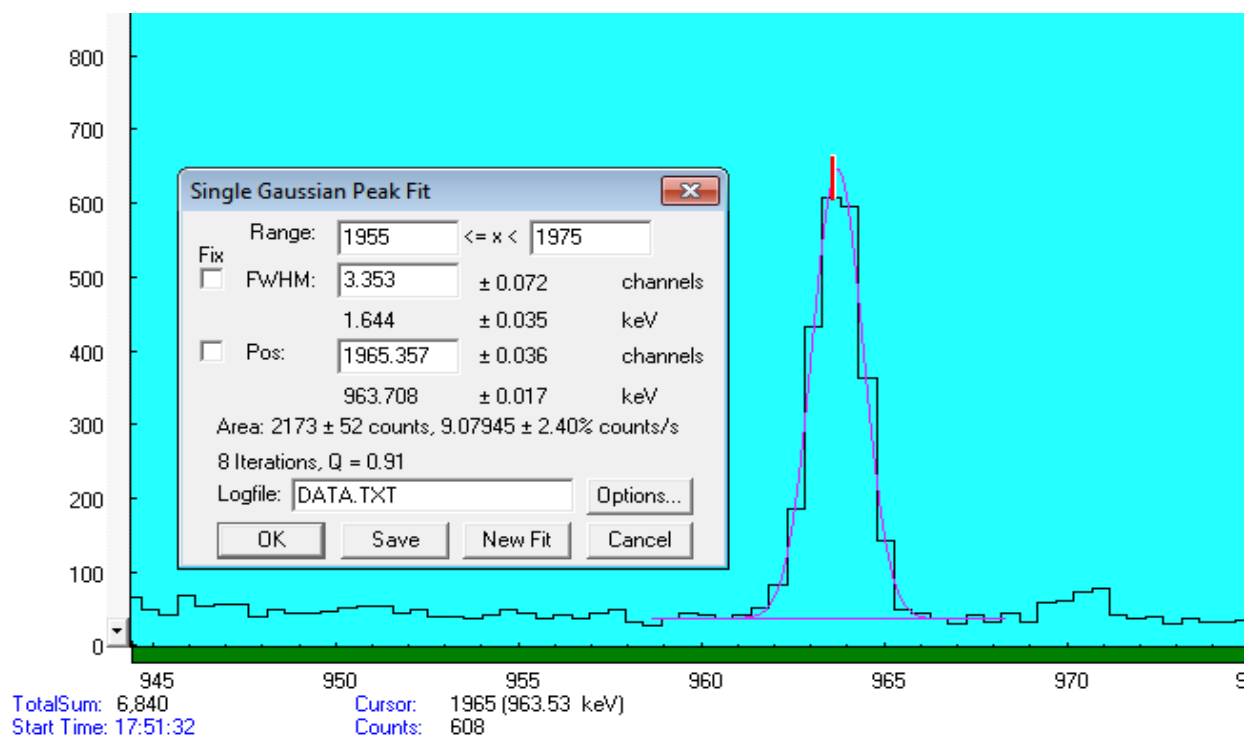


Fig. 17: Coal ash A3, 2 hours after beam off, 239s count time.

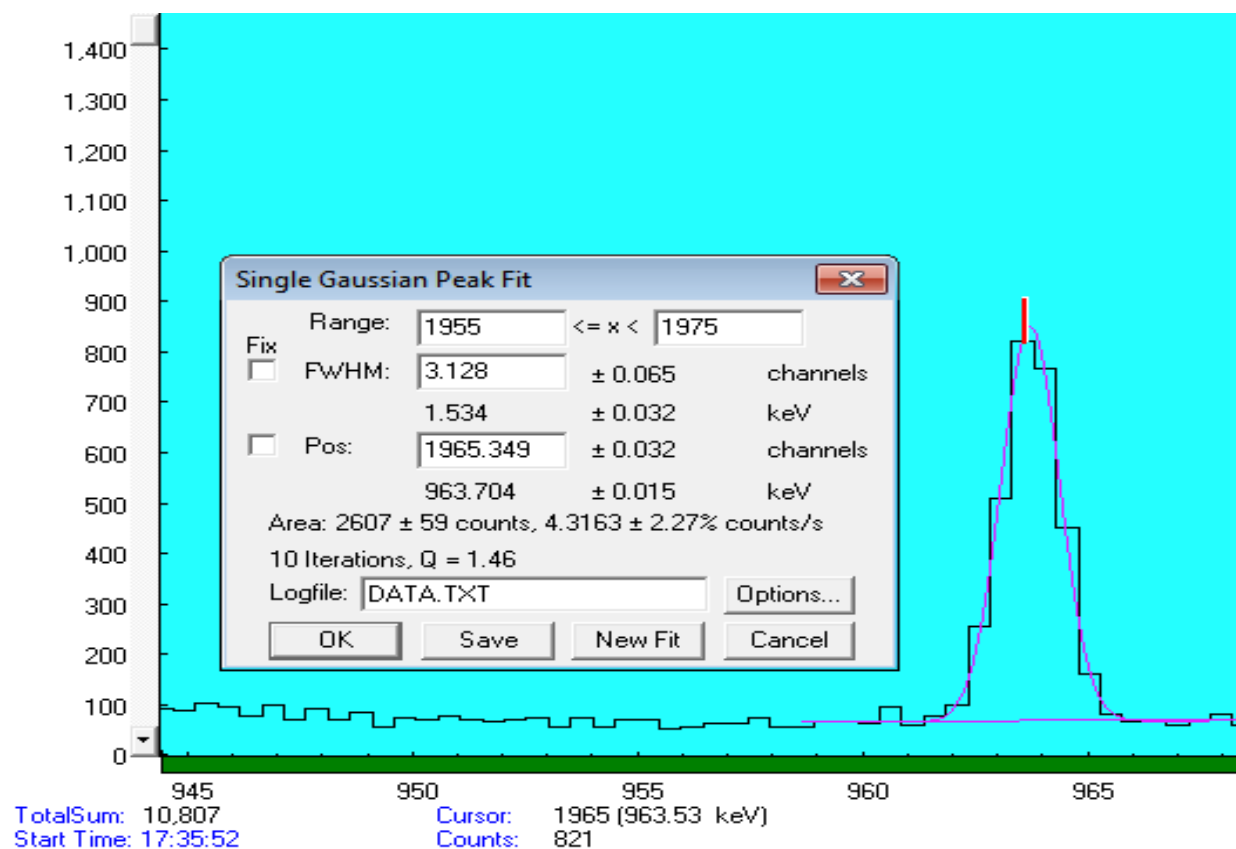


Fig. 18: Coal ash A2, 1.5 hours after beam off, 604s count time.

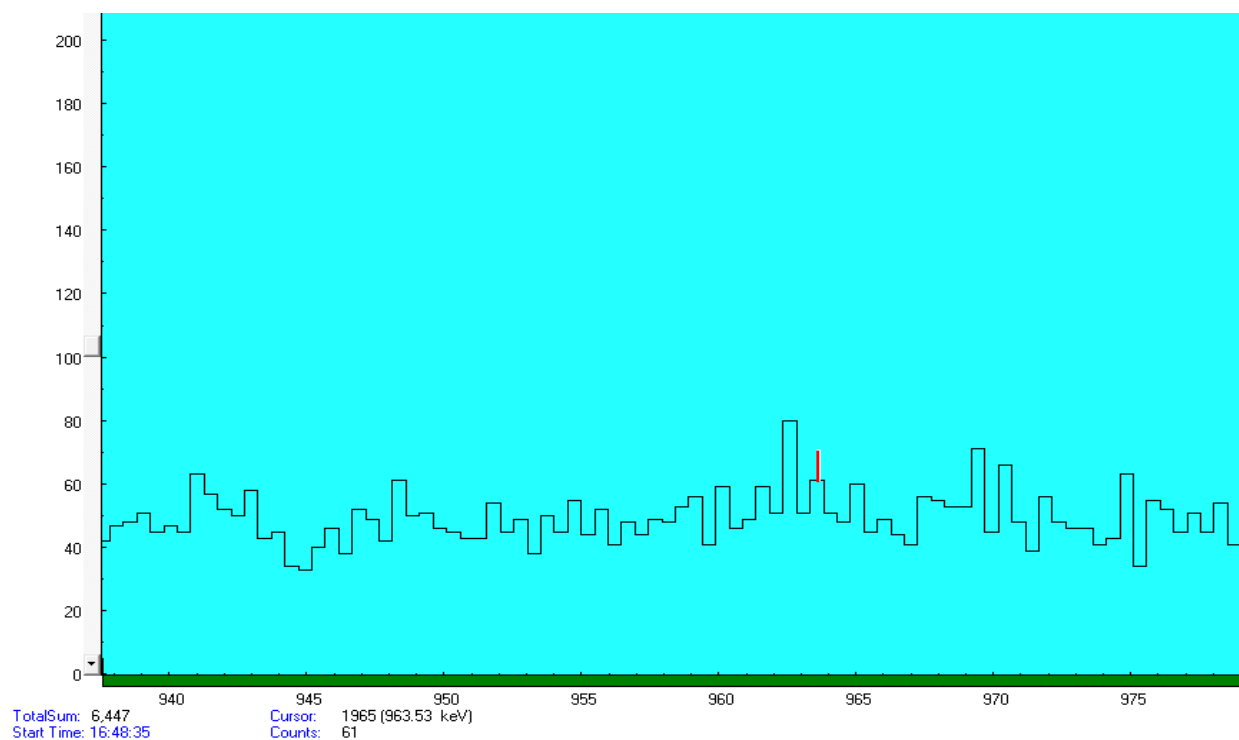


Fig. 19: Coal ash A1, 1 hour after beam off, 1228s count time; no 963 keV signal.

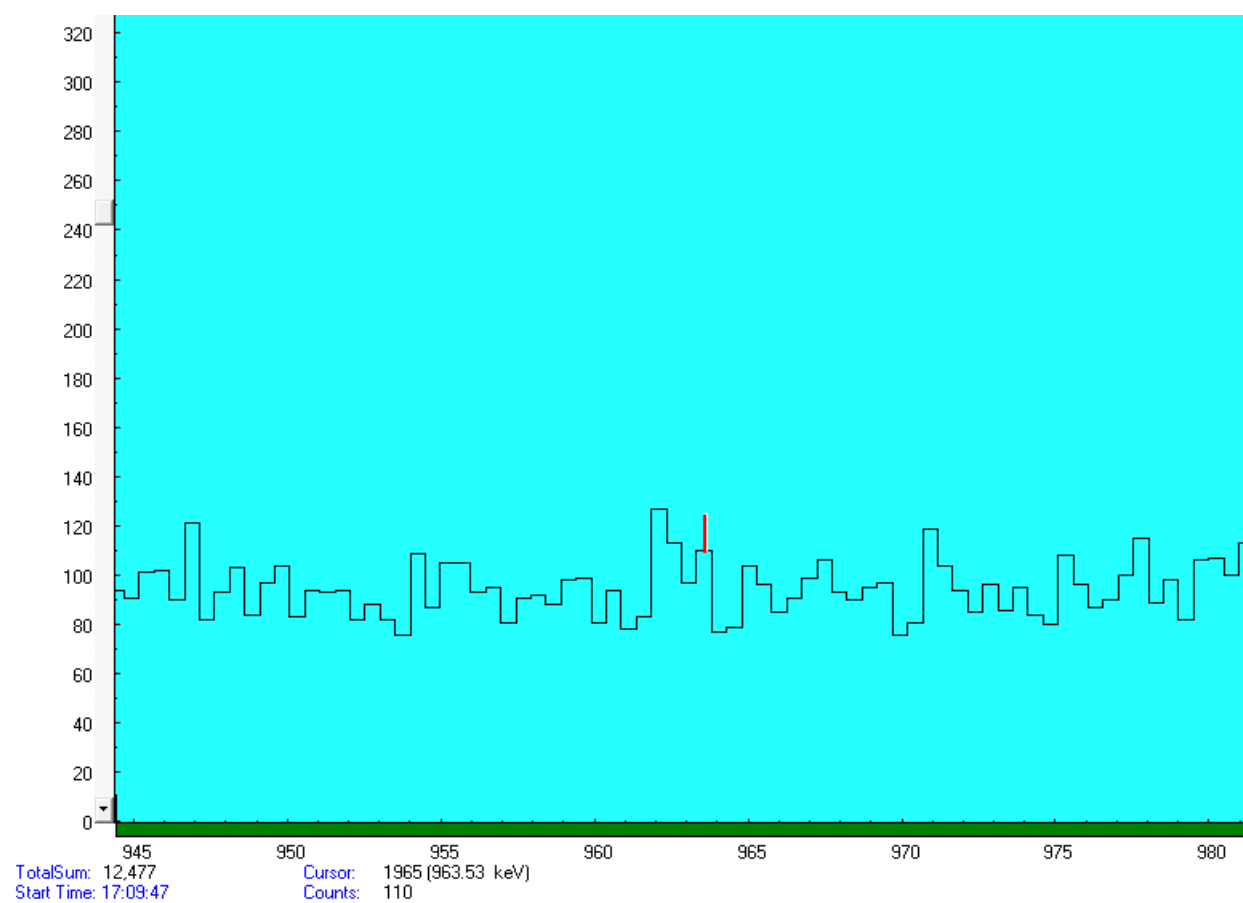


Fig. 20: Coal Ash A1, 1 hour after beam off, 1318s count time; no 963 keV signal.

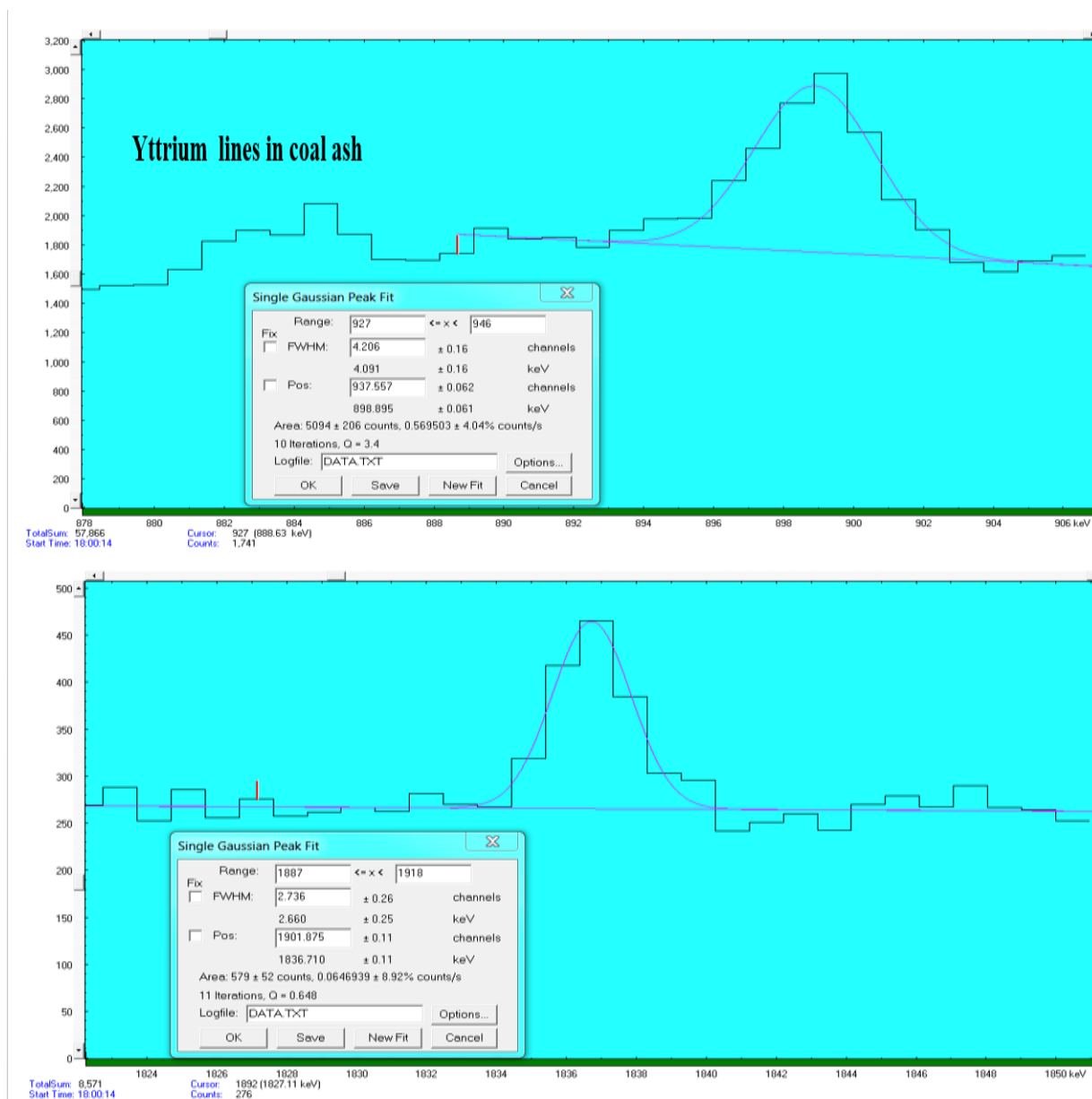


Fig. 21: Dr. Dale's coal ash run 12 (using 898keV since it is more dominant).

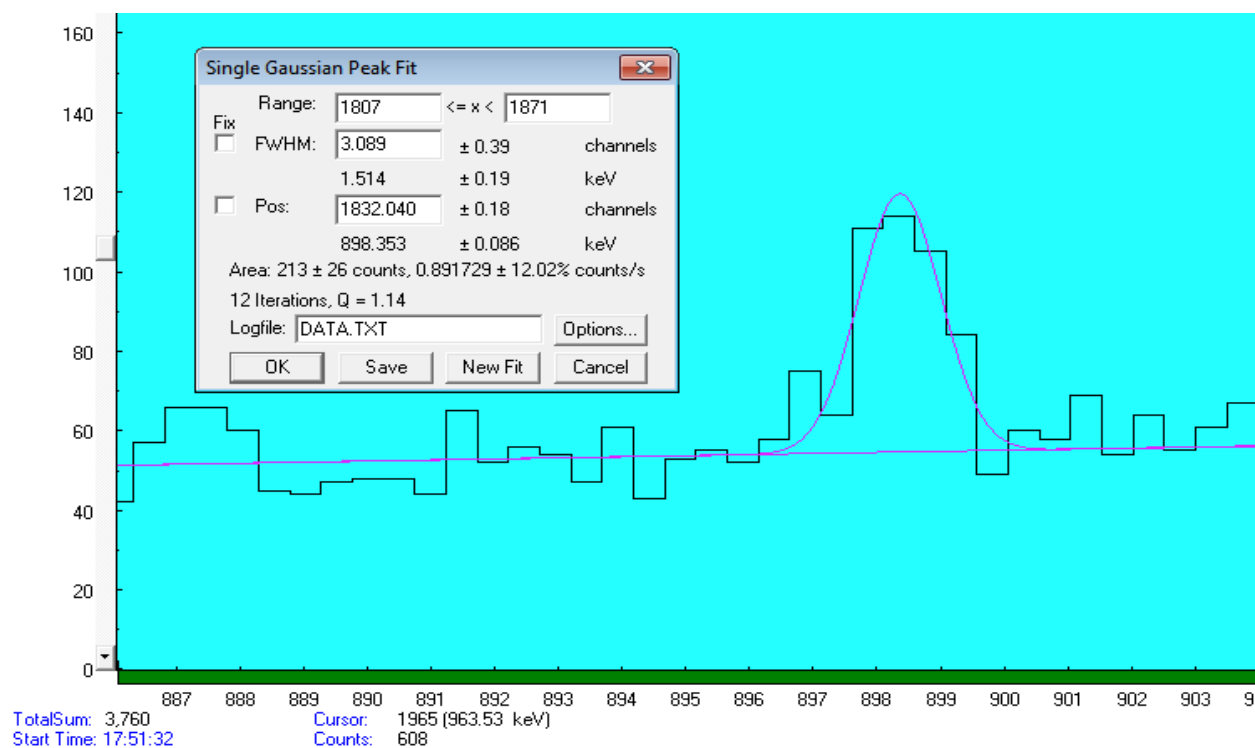


Fig. 22: Coal ash A3, 2 hours after beam off, 239s count time.

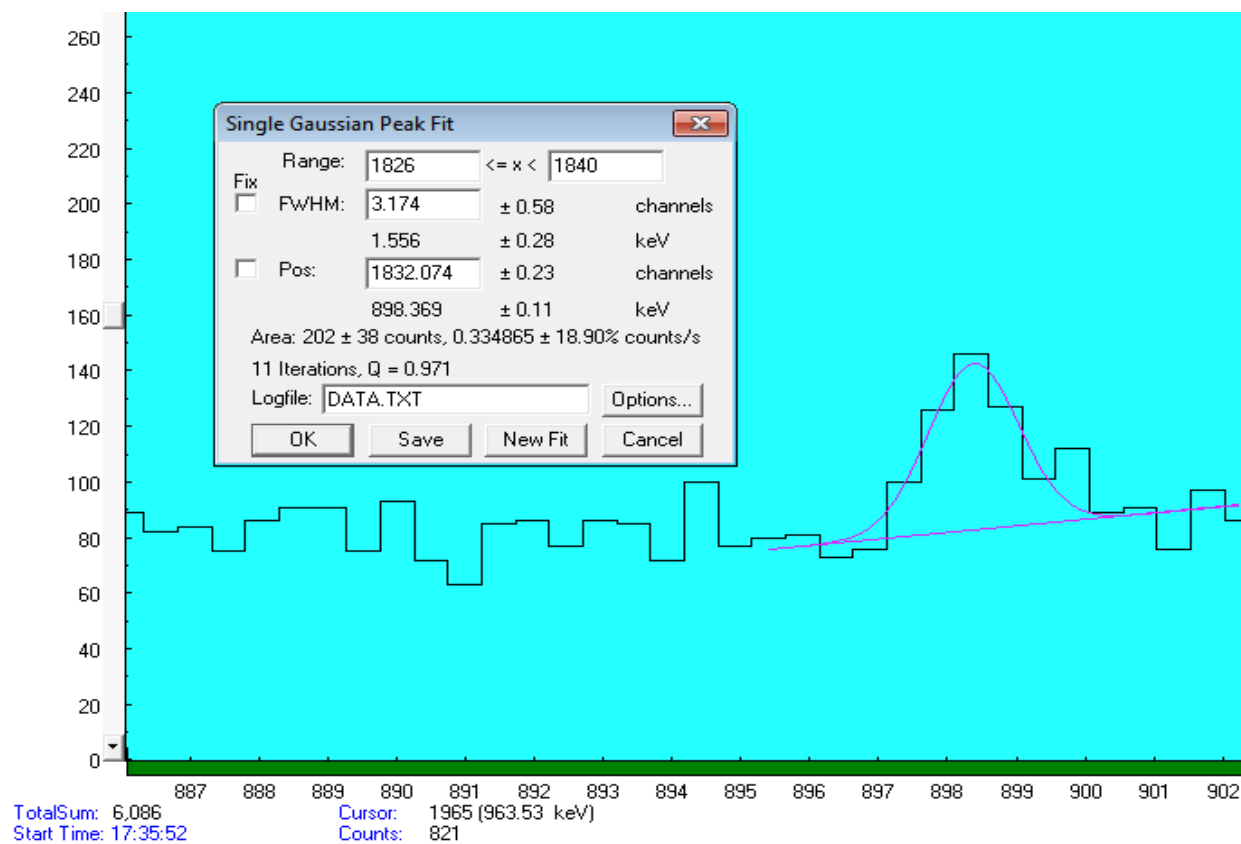


Fig. 23: Coal ash A2, 1.5 hours after beam off, 604s count time.

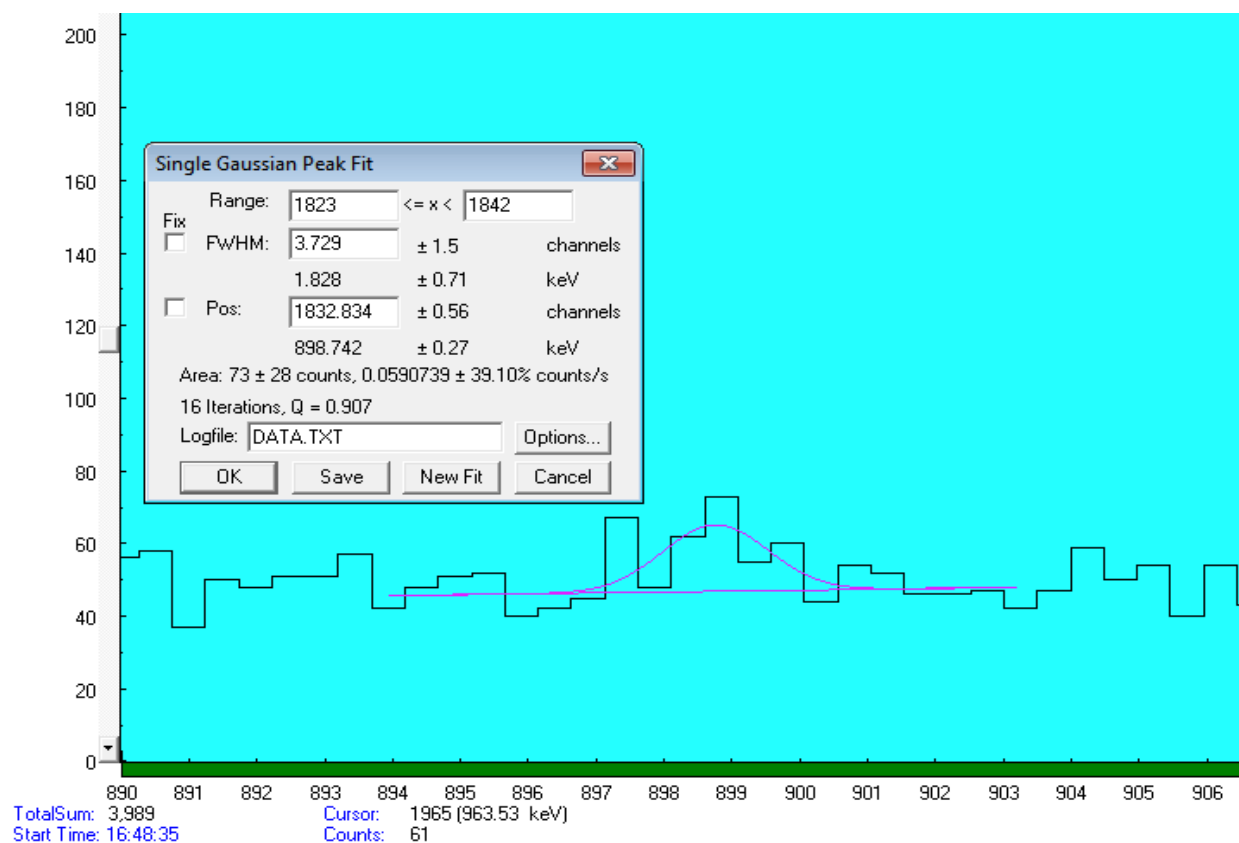


Fig. 24: Coal ash A1, 1 hour after beam off, 1228s count time.

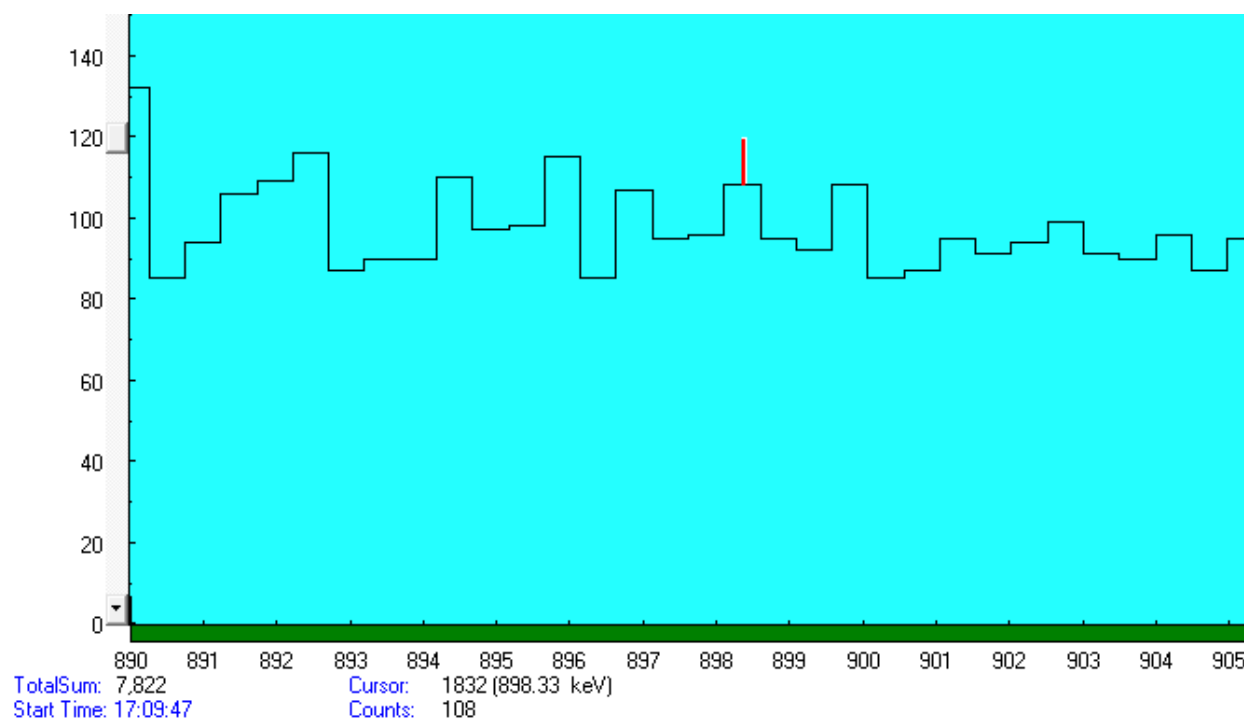


Fig. 25: Coal ash A1, 1.5 hours after beam off, 1318s count time; no 898 keV signal.

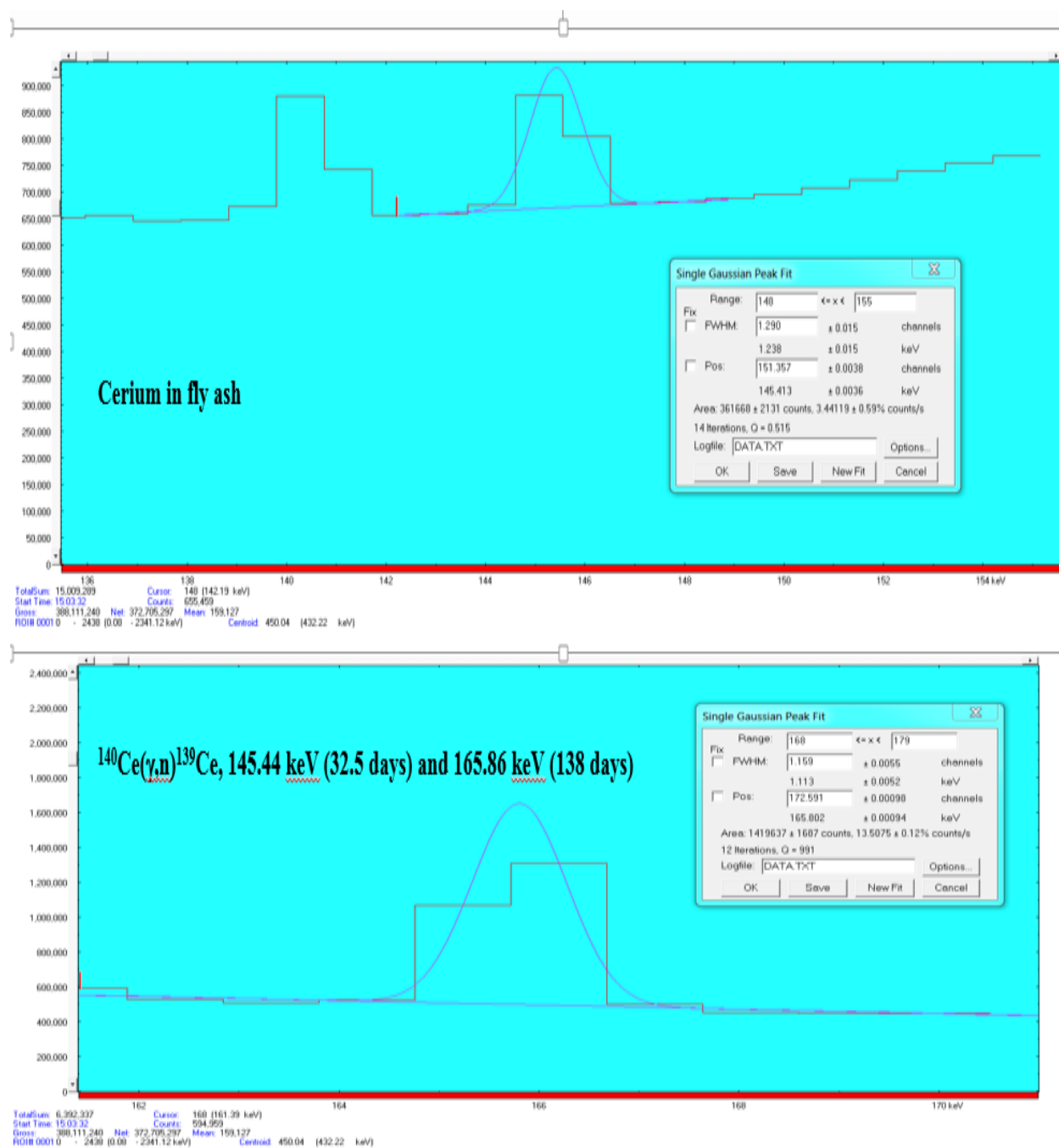


Fig. 26: Dr. Dale's fly ash run 20.

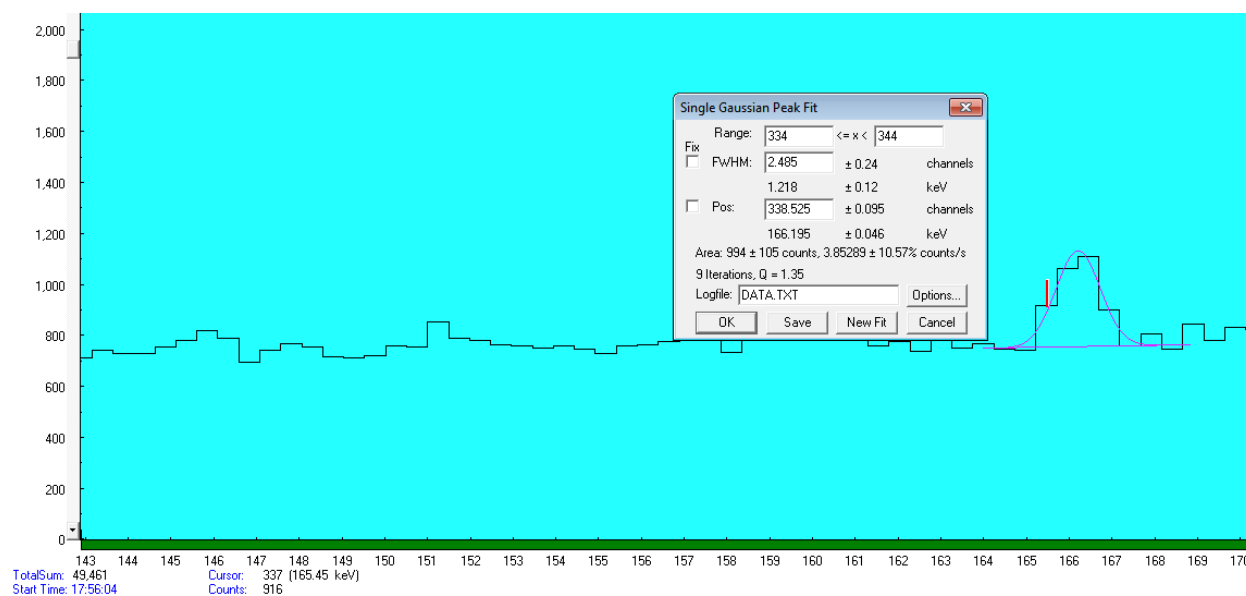


Fig. 27: Fly ash F3, 2 hours after beam off, 258s count time.

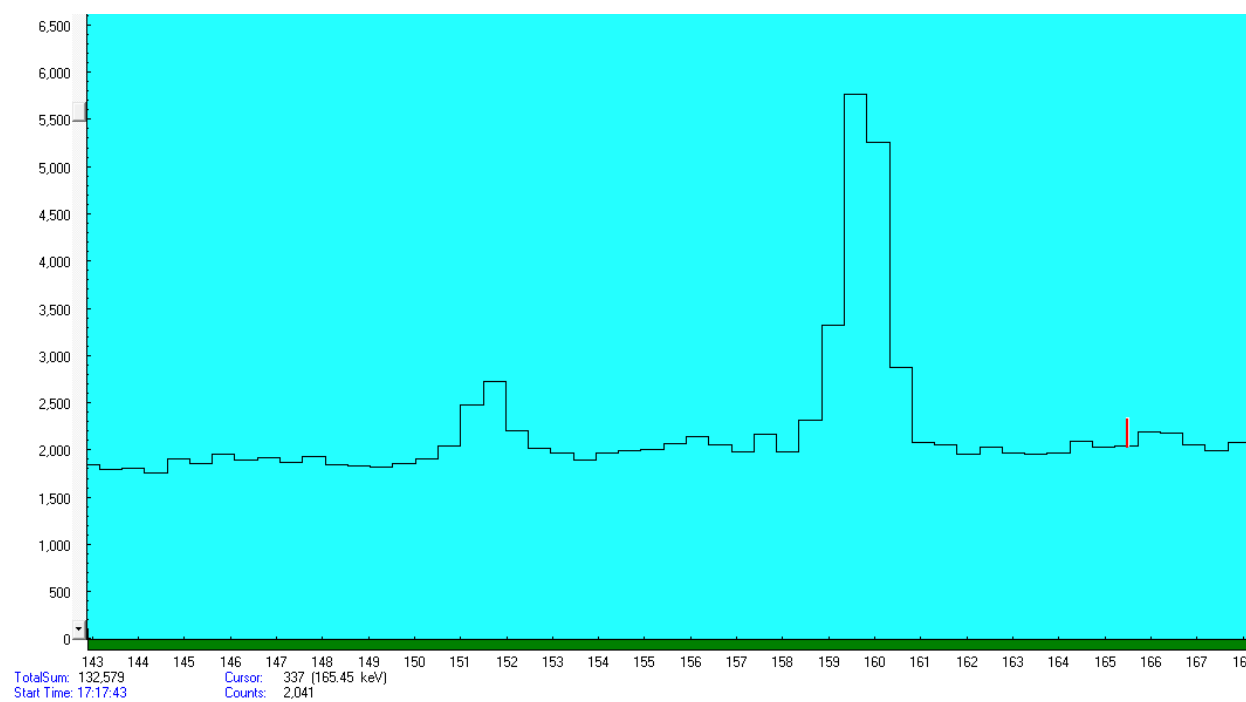


Fig. 28: Fly ash F2, 1 hour after beam off, 2266s count time; no 145 or 166 keV signal.

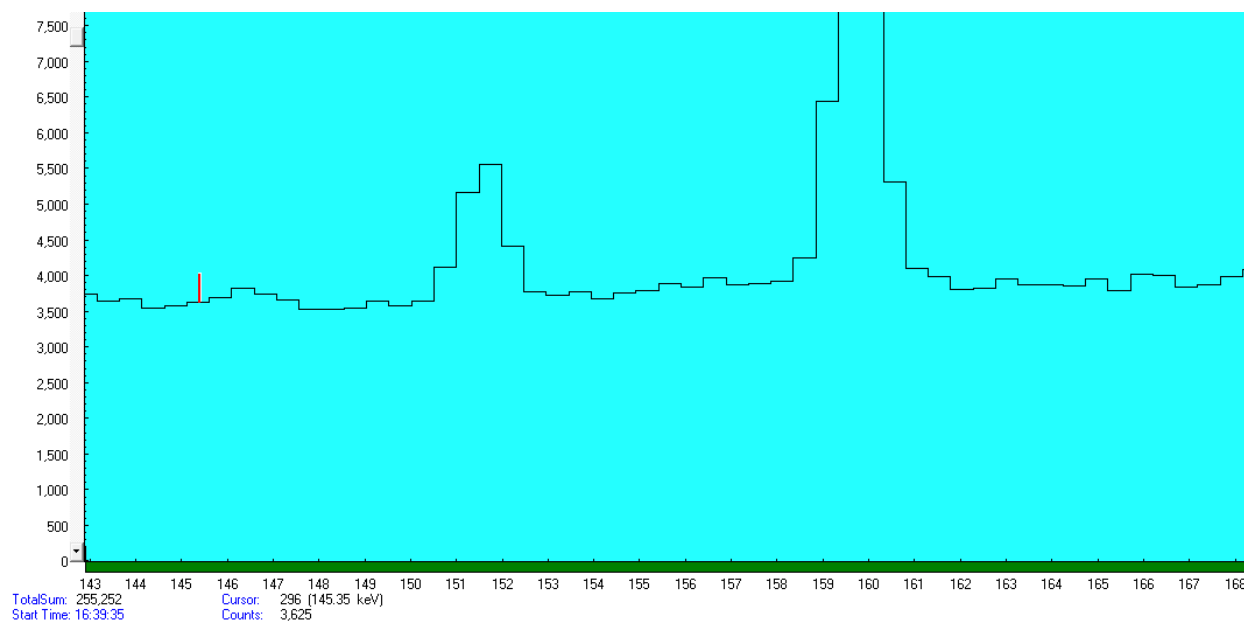


Fig. 29: Fly ash F1, 30min after beam off, 2223s count time; no 145 or 166 keV signal.

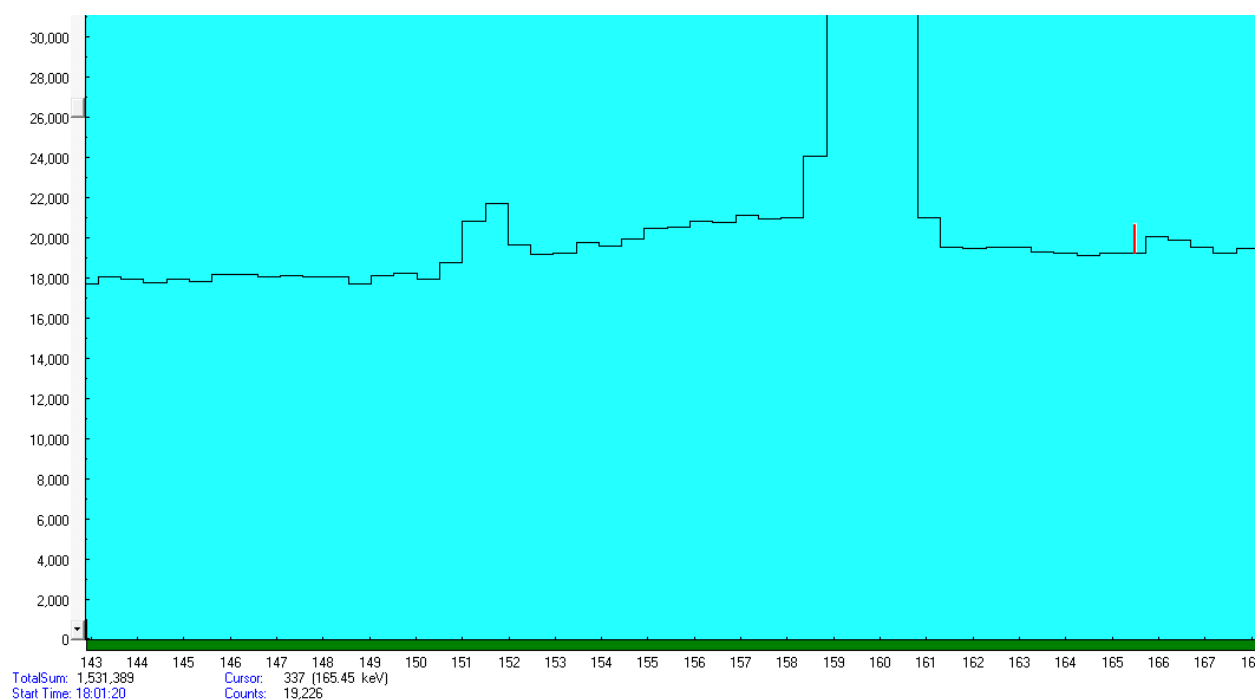


Fig. 30: Fly ash F1, 2 hours after beam off, 47641s count time; no 145 or 166 keV signal.

Chapter 5

Conclusions

5.1 Slag Conclusions

The mining slag does contain trace amounts of scandium (17.4 ± 2.0 ppm) and yttrium (255.2 ± 1.9 ppm); however, this does not prove that it does not contain the other rare earth elements of interest. The slag may contain those elements at levels below the detectable limit of the experiment. The line from praseodymium was much too faint to see with this approach; a future experiment might use higher energies to increase the flux received or to excite a different reaction. The 165 keV cerium and 963 keV europium signals are faintly measurable in sample D indicating that the reactions were occurring. The small size of the signals from sample D, which had the largest spike added, implies that the concentrations of europium in slag are below the detection limit of this experiment.

The uncertainties in all calculations are created by using the propagation of errors method. The errors used for this method are the ± 0.00005 g of the scale used to measure all of the masses, as well as the counting percent errors provided by the MPA program.

5.2 Coal, Coal Ash and Fly Ash Conclusions

The count data from C2 is missing due to a corruption of the save file. This missing data means the uncertainty in the calculated value should be higher. The data indicate that scandium is present in all of the samples studied. The yttrium signal in the coal ash has a large error due to the propagation of a 39% counting error in sample A1. This error is due to the very small activity and concentration of the yttrium as well as the inability to take long counts. It would appear from the

data that the scandium is deposited in the coal ash and the fly ash fairly evenly. The data indicate that yttrium is volatilized and deposited in the fly ash with an increased concentration.

According to the USGS a sample of coal from the Mary Lee coal bed in Walker County, Alabama has a scandium concentration of 5.1 ppm [10]. The value from the USGS has very good agreement with the experimental value of 4.9 ± 0.1 , the values are not in perfect agreement due to the variable makeup of coal. The USGS sample also contained 0.47 ppm of europium and 5.9 ppm of yttrium. Those elements were not detected in the coal samples directly but they were detected in the more concentrated coal ash and fly ash.

In a study done by the Department of Civil and Environmental Engineering in collaboration with the Center for Applied Energy Research and Duke University samples of coal combustion products from several power plants were analyzed. In the study the scandium content of fly ash was 30.29 ± 7.22 . This value is lower than the calculated value of 54.22 ± 0.58 , but this could be due to the variability of the parent coal.

5.3 Missing Elements Conclusions

This experiment was focused on a broad spectrum approach to help validate the efficacy of PAA. All of the elements added to the samples by spiking them were detected except for one. This indicates that the technique applied for detecting them was valid, but that a more precise attempt is needed. The precision could be increased by focusing on a specific element and tuning the parameters of the experiment to fit that element. The parameters tuned could include irradiation time, count time, cooldown time, and beam energy.

The cerium in slag is the only rare earth element that did not show gamma lines in the spiked samples. This seems to imply that the concentration of cerium was below the minimum detectable limit, or that the cross section for the reaction was too small. The calculated threshold energy for the reaction is 9.2 MeV meaning the bremsstrahlung flux contained photons above the reaction energy threshold. It would appear that this experiment was not a successful technique for detecting cerium in these samples. However, a different experimental setup and parameters could allow PAA to detect cerium.

References

- [1] Segebade, C., Weise, H., & Lutz, G. J. (1988). *Photon activation analysis* (Vol. 2). Berlin: De Gruyter.
- [2] Dams, R. (1992). Nuclear Activation Techniques for the Determination of Trace Elements in Atmospheric Aerosols, Particulates and Sludge Samples. *Internation Union of Pure and Applied Chemistry*, 64(7), 991-1014. Retrieved from <https://www.iupac.org/publications/pac/pdf/1992/pdf/6407x0991.pdf>
- [3] Nuclear Data Center at KAERI. (n.d.). Retrieved from <http://atom.kaeri.re.kr/>
- [4] National Nuclear Data Center. (n.d.). Retrieved from <https://www.nndc.bnl.gov/>
- [5] I. Olmez and N.K. Arm, J. Radioanal. Cbem., 2, 671 (1977).
- [6] J.M. Ondov, W.H. Zoller, I. Olmez, N.K. Aras, G.E. Gordon, L.A. Rancitelli, K.M. Abel, R.H. Filby, K.R. Shah and R.C. Ragaini, Anal. Cbem., 47, 4102 (1975).

- [7] Sun, Z. J., Segebade, C., Wells, D., Maschner, H., Benson, B., & Cole, P. L. (2011, January). Determination of Trace Elements in Coffee by Photon Activation Analysis. Retrieved from https://www.researchgate.net/profile/Z_Sun4/publication/289018892_Determination_of_trace_elements_in_coffee_by_photon_activation_analysis/links/568a79c408ae1e63f1fbcb8a8/Determination-of-trace-elements-in-coffee-by-photon-activation-analysis.pdf
- [8] Mamtimin, M., Cole, P. L., & Segebade, C. (2011, January). Proof - of - Principle Results for Identifying the Composition of Dust Particles and Volcanic Ash Samples through the Technique of Photon Activation Analysis at the I AC. Retrieved from https://www.researchgate.net/profile/Mayir_Mamtimin/publication/289297705_Photon_activation_analysis_of_dust_particles_for_environmental_research_and_applications_using_the_44-MeV_electron_linac_at_the_Idaho_Accelerator_Center/links/56901b7908aec14fa557d5ca/Photon-activation-analysis-of-dust-particles-for-environmental-research-and-applications-using-the-44-MeV-electron-linac-at-the-Idaho-Accelerator-Center.pdf
- [9] Lutz, G. J. (1971). Photon Activation Analysis-A review [Abstract]. *Analytical Chemistry*, 43(1), 93-103. Retrieved from <https://pubs.acs.org/journal/ancham>.
- [10] Schweinfurth, S. P. (2016, November 23). Coal—A Complex Natural Resource. Retrieved from <https://pubs.usgs.gov/circ/c1143/html/text.html#tab4>

- [11] Huggins, F. E., Shah, N., Zhao, J., Lu, F., & Huffman, G. P. (1993). Nondestructive determination of trace element speciation in coal and coal ash by XAFS spectroscopy. *Energy & Fuels*, 7(4), 482-489. doi:10.1021/ef00040a008
- [12] Ekmann, J. M. (2012). Rare Earth Elements in Coal Deposits – a Prospectivity Analysis. *Search and Discovery*, 80270th ser., 1-40. Retrieved from <http://www.searchanddiscovery.com/>
- [13] Taggart, R. K., Hower, J. C., Dwyer, G. S., & Hsu-Kim, H. (2016). Trends in the Rare Earth Element Content of U.S.-Based Coal Combustion Fly Ashes. *Environmental Science Technologies*, (50), 11th ser., 5919-5926. doi:10.1021/acs.est.6b00085
- [14] Engels, J. (n.d.). Tailings.info. Retrieved from <http://www.tailings.info/basics/tailings.htm>
- [15] Coil, D., Lester, E., Higman, B., & Mattox, A. (2010, December 15). Mine Tailings. Retrieved from <http://www.groundtruthtrekking.org/Issues/MetalsMining/MineTailings.html>
- [16] Economics of Nuclear Power. (2017, December). Retrieved March 25, 2018, from <http://www.world-nuclear.org/information-library/economic-aspects/economics-of-nuclear-power.aspx>

- [17] Knapp, A. (2012, July 11). How Much Does It Cost To Find A Higgs Boson? Retrieved March 25, 2018, from <https://www.forbes.com/sites/alexknapp/2012/07/05/how-much-does-it-cost-to-find-a-higgs-boson/#64bff5839480>
- [18] What Are Technology Metals? (n.d.). Retrieved March 25, 2018, from <http://www.techmetalsresearch.com/what-are-technology-metals/>
- [19] U.S. Energy Information Administration - EIA - Independent Statistics and Analysis. (n.d.). Retrieved March 25, 2018, from <https://www.eia.gov/coal/production/quarterly/>
- [20] Yeung, J. (n.d.). Bremsstrahlung | Radiology Reference Article. Retrieved March 25, 2018, from <https://radiopaedia.org/articles/bremsstrahlung>
- [21] Bremsstrahlung. (n.d.). Retrieved March 25, 2018, from <http://www.radioactivity.eu.com/site/pages/Bremsstrahlung.htm>
- [22] Overcoming the Coulomb Barrier. (n.d.). Retrieved March 25, 2018, from <http://burro.cwru.edu/academics/Astr221/StarPhys/coulomb.html>

- [23] Spicer B.M. (1969) The Giant Dipole Resonance. In: Baranger M., Vogt E. (eds) Advances in Nuclear Physics. Springer, Boston, MA
- [24] Shizuma, T. (n.d.). Strength Distribution of Dipole Excitation [Slide 5]. Retrieved March 25, 2018, from <http://slideplayer.com/slide/3367782/>
- [25] Sprawls, P. (n.d.). INTRODUCTION AND OVERVIEW. Retrieved March 26, 2018, from <http://www.sprawls.org/ppmi2/RADIOTRANS/>

Appendix A: Python Code

```
import ROOT
```

```
import numpy as np
```

```
xs = [[2.3106,33.09],[0,1.9574,23.463]]
```

```
ys = [[0.061,0.112],[0.0016, 0.02331, 0.055]]
```

```
errxs = [[0.14,0.14],[0,0.14,0.14]]
```

```
errys = [[0.00136,0.00266],[0.0006,0.0041,0.00795]]
```

```
xtitles = ["spike mass [mg]"]*2
```

```
ytitles = ["cps"]*2
```

```
titles = ["Decay Corrected Counts/Sec per Sample Mass Vs Spike per Sample Mass"]*2
```

```
N=map(int,[np.sqrt((-10+1000/10*10/10*10+10)**2))][0]
```

```
grs=[]
```

```
canvuuuuuus = ROOT.TCanvas()
```



```
_g_.Fit("pol1")
```

```
_g_.SetTitle(title)
```

```
_g_.GetXaxis().SetTitle(xtitle)
```

```
_g_.GetYaxis().SetTitle(ytitle)
```

```
ROOT.gStyle.SetOptFit(int("1011"));
```

```
grs.append(_g_)
```

```
_g_.Draw("*A")
```

```
i+=1
```

```
#?
```

```
grs[-1].GetYaxis().SetRangeUser(0,0.07)
```

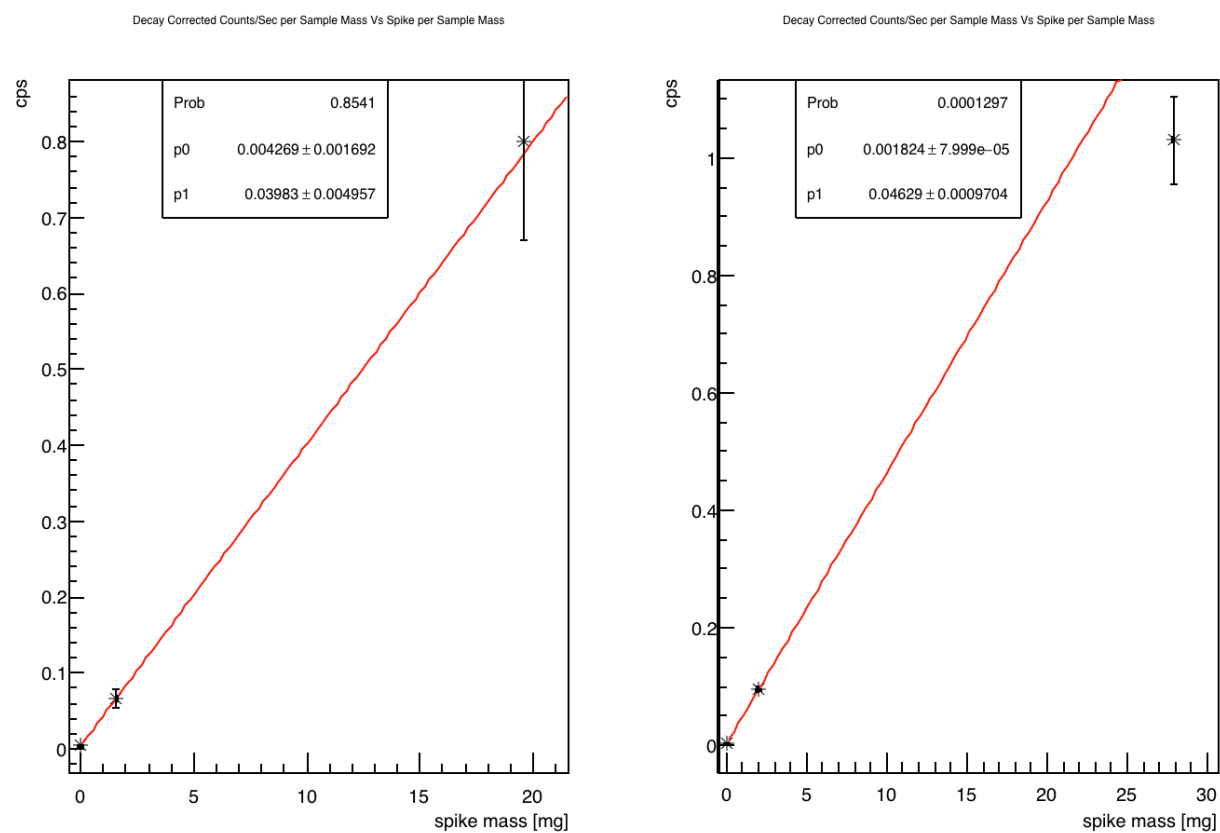
```
grs[0].GetYaxis().SetRangeUser(0,0.12)
```

```
grs[-1].GetXaxis().SetLimits(-3,26)
```

```
_g_.GetXaxis().SetTitle(xtitle)
```

```
canvuuuuus.Draw()
```

Appendix B: Python Graphs



Python fit graphs with yttrium in coal ash on left, and scandium in coal ash on the right.